Experimental Verification and Development of

Structural Identification Techniques on a Grid

by

Steven Phillip Kahn

Thesis submitted to the Faculty of the

Virginia Polytechnic Institute and State University

in partial fulfillment of the requirements for the degree of

Master of Science

in

Engineering Mechanics

APPROVED:

Mark A. Norris, Chairman

Leonard Meirovitch

Dean T. Mook

April, 1990

Blacksburg, Virginia

Experimental Verification and Development of

Structural Identification Techniques on a Grid

by

Steven Phillip Kahn

Mark A. Norris, Chairman

Engineering Mechanics

(ABSTRACT)

The work that is reported herein deals with system identification methods for large flexible structures. Proposed space missions for the future include the deployment of large flexible structures, e.g., NASA's proposed space station. These structures must be controlled to maneuver the structure to desired locations and to suppress unwanted vibration. Before controlling any structure, it is necessary to have an accurate model which may include accurate estimates of the structure's natural frequencies and mode shapes. System identification is an important process that precludes system control. Precision structures such as those proposed for the Space-Based Laser or the Aerospace Plane require high performance control systems which will require robust, computationally efficient system identification algorithms. This work attempts to experimentally verify, develop, and compare existing identification algorithms to determine their properties and improve their efficiency towards potential applicability in a space environment. To this end, we consider the Temporal Correlation Method and the Eigensystem Realization Algorithm. The algorithms are implemented on the Astronautics Laboratory Grid structure, and the results of the algorithms are compared in the presence of damping, noise, and residual modes. In addition, the Temporal Correlation Method is shown to be a constrained version of the Eigensystem Realization Algorithm for cases of light damping.

Acknowledgements

I would like to take this opportunity to express my gratitude to various individuals who were a help to me in completing this research. First of all, much thanks and appreciation are due to my major advisor Dr. Mark A. Norris. His guidance and leadership throughout this year have been immeasurable. Also, I would like to thank Dr. Alok Das of the Astronautics Laboratory at Edwards Air Force Base for his ideas and support. In addition, I find it necessary to express my gratitude to Waid Schlaegel, also at the Astronautics Laboratory, for all the help he has provided me. Finally, I would like to thank my wife, Buff, for her support, understanding, and encouragement. Without her I'm not sure if I would have made it.

Table of Contents

List of Illustrations

List of Tables

1 Introduction

1.1 Purpose and Scope

The study of large space structures has received considerable interest recently. These structures can be characterized as being lightly-damped, nearly self-adjoint distributed structures. Control of large flexible structures requires accurate knowledge of the system parameters, e.g., natural frequencies, mode shapes, mass, damping, and stiffness properties. Hence, system identification is a prerequisite to system control. Proposed space missions for the near future, e.g., NASA's space station, will require control for accurate maneuver and vibration suppression. These structures may be incapable of supporting their own weight in a 1-G environment. In the case in which ground-based testing of the fully deployed structure is not possible, a robust, computationally- efficient identification algorithm must be implemented on-orbit. To test and evaluate the identification techniques, ground tests must be performed to determine their practicality, performance, and robustness.

Practical limitations require the discretization of the mathematical model describing the structure in which only a finite number of modes can be modeled. If certain modes participate in the system's response but are not modeled, we call them residual modes. The effect of the residual modes on the identified parameters is called identification spillover. Analogously, the excitation of residual modes caused by the controller is known as control spillover. Both identification and control spillover tend to degrade system performance.

In addition to identification spillover, there are other factors that can affect the performance of the identification methods. Two of these factors are damping in structures, which tends to behave nonlinearly in actual systems, and the amount of noise in the sensor output. An examination of these elements of error is important in the overall evaluation of any identification technique. For an actual physical system it would be difficult, if not impossible, to distinguish between spillover error, damping error, and noise error. Therefore, it is necessary to test the methods using computer simulations so that each error may be individually analyzed. Once the simulations have been completed and an error analysis has been performed, the method is tested on a physical system. Any error found for the identified results of the physical system can now be better understood based on the simulation studies.

The objective of this research was to experimentally verify, compare, and improve existing structural identification techniques, focusing on those which are suitable for on-orbit application. The identification techniques will be tested using computer simulations along with a ground-based experiment, namely the Astronautics Laboratory Grid structure. We consider two identification algorithms: (1) the Temporal Correlation Method (TCM) and (2) the Eigensystem Realization Algorithm (ERA). The TCM uses the temporal correlation and spatial orthogonality properties of lightly-damped, nearly self-adjoint distributed structures, and the estimates of the eigenvalues and eigenvectors

are obtained through the solution of an algebraic eigenvalue problem. The matrices used in the algebraic eigenvalue problem are found by correlating sensor measurements. The ERA begins by forming the generalized Hankel matrix consisting of free or impulse response measurements. The singular value decomposition of the Hankel matrix is used to obtain a minimum-order realization of the system. Modal identification is then performed by solving an algebraic eigenvalue problem involving the realized transition matrix. The TCM is implemented in the configuration space while the ERA is implemented in the state space. In particular, the ERA modal identification is performed by solving a $2n^{(th)}$-order eigenvalue problem while the TCM modal identification is performed by solving an $n^{(th)}$-order eigenvalue problem. It is shown in the sequel that the TCM reduces to a constrained version of the ERA in cases of light damping. This is significant because it reduces the number of computations in the ERA, and hence, improves the efficiency of the algorithm.

The research presented herein provides the theoretical background for the TCM, the ERA, and the constrained ERA (CERA). These methods are tested using computer simulations to determine their performance in the presence of damping and noise. In addition, the effect of identification spillover is examined. The TCM and the ERA are then implemented on the Astronautics Laboratory Grid structure, located at Edwards Air Force Base in Edwards, California.

1.2 Literature Review

Identification methods are either carried out in the frequency domain or the time domain. Early schemes were implemented in the frequency domain. Frequency domain

methods, however, have been shown to suffer from high levels of damping and from closely space frequencies. This is attributed to modal interference of the closely spaced frequencies. Because of these limitations, the focus now is on the time domain.

Early time domain methods included the least-squares curve-fitting time domain method. Caravani, Watson, and Thomson presented a recursive least-squares formulation to identify physical parameters of a structure [1]. They used an *N*-dimensional building to demonstrate the method which assumes prior knowledge of a lumped-mass model to identify damping and stiffness parameters. The approach uses the Kalman filter equations to update the estimates as new data becomes available. Another least-squares technique, developed by Smith, is a time domain method that identifies frequencies, damping values, and participation factors from free-response data [2]. The method represents an extension of previous methods [3,4] and makes improvements in several areas. First, the amount of computer time is substantially reduced. Second, the method can handle noisy data containing many modes. Thirdly, the method makes use of the fast Fourier transform of the raw data to provide initial estimates of the parameters, thereby reducing the need for user input. Finally, the method allows for the possibility of using multiple data sets to improve the accuracy of the results.

Another time domain method is the Ibrahim Time Domain (ITD) method [5,6]. It is a modal identification technique implemented in the state space and is applicable to both lumped and distributed parameter systems. Furthermore, the data used can be displacements, velocities, or accelerations. The method was demonstrated using a cantilever beam with good results, and the method was shown to be insensitive to measurement noise.

Juang and Pappa have written many papers dealing with yet another time domain method called the Eigensystem Realization Algorithm (ERA) [7-13]. The ERA uses a generalized Hankel matrix consisting of free or impulse response data. The singular

value decomposition of the generalized Hankel matrix at $t = 0$ is used to form a $2n$ x $2n$ algebraic eigenvalue problem, where n is the number of identified modes [7]. In addition, the Hankel matrix allows for multiple data sets which enables the identification of repeated eigenvalues. The method has been tested on data from the Galileo spacecraft modal survey test with approximately 30 modes being identified [8]. The ERA also introduces two accuracy parameters referred to as Modal Amplitude Coherence and Modal Phase Collinearity. These parameters give a quantitative measure of the accuracy of the identified quantities.

Juang and Pappa have studied the influence of noise on modal parameters identified by the ERA [9] and determined an optimum singular value cutoff in the case in which the covariance of the noise is known. In addition, they developed an Eigensystem Realization Algorithm using data correlations (ERA/DC) [10] in an attempt to reduce the effect of noisy data. The method is tested using a simulated five-degree-of-freedom system. The impulse responses are corrupted with 2% measurement noise. The results indicate that the ERA/DC can reduce bias due to noise without model overspecification. Finally, an ERA formulation in the frequency domain has been performed [11]. In addition, a mathematical formulation of the relationship between time domain and frequency domain modal identification is presented.

Montgomery and others have used Autoregressive Moving Average (ARMA) models to identify control effectiveness parameters of a structure [14-17]. A least square parameter identification algorithm identifies the control coefficients of the second-order difference equation obtained for each mode. The frequency and damping ratio for each mode is predetermined from free-decay tests. The method has been tested on a highly flexible grid [14] and was improved by correcting for the resonant frequency of each mode through the observed beating in the records [15]. Additional tests have been made using the Spacecraft Control Laboratory Experiment (SCOLE) [16,17].

Baruh and Meirovitch introduced a physical parameter identification technique that makes use of the identified eigensolutions of the actual distributed system to identify mass and stiffness distributions [18]. The method expands the mass and stiffness distributions in a finite series of known spatial functions multiplied by unknown coefficients. Then, the least squares method, along with the orthogonality conditions of the eigenfunctions, are used to identify the undetermined coefficients. Meirovitch and Norris have developed physical parameter identification methods based on the finite element method using both the time and frequency domains [19,20]. The object is to identify average values of mass, damping, and stiffness distributions over each element. The approach is demonstrated using a free-free nonuniform beam [19] and an undamped cantilever beam in bending vibration [20] where in the latter a perturbation approach is used.

Another modal identification technique, developed by Norris and Silverberg, uses the temporal correlation and spatial orthogonality properties of lightly-damped, nearly self-adjoint distributed structures and is called the Temporal Correlation Method (TCM) [21,22]. The continuous eigenvalue problem is reduced to an algebraic one in which the eigenvalues and eigenvectors are related to the natural frequencies and mode shapes of the distributed system. In addition, the identified frequencies obey the inclusion principle. The method has been tested using a steel cantilever beam and an aluminum grid structure with good results. Degradation of the identified values occurs because of noise in the sensors, damping in the response, and identification spillover. Hedgecock provides an experimental verification of the TCM along with a study of key parameters [23].

Norris demonstrates that the TCM reduces to a constrained version of the ERA for cases of light damping [24]. The method uses only one row of block matrices containing the impulse response to form the generalized Hankel matrix. The result is that the order of the eigenvalue problem used to obtain the modal quantities is reduced by a factor of

two, thereby improving the efficiency of the algorithm. The method is tested using computer simulations of a simply supported beam and a membrane. Good results are obtained for light levels of damping.

3 The Temporal Correlation Method

3.1 Equations of Motion

The governing equation of motion of a lightly-damped distributed structure is given by the partial differential equation (pde)

$$\mathscr{L}u(P,t) + \zeta\dot{u}(P,t) + m(P)\ddot{u}(P,t) = f(P,t),\ P \in D \tag{1}$$

where $u(P,t)$ is the displacement at the spatial position P at time t, $\mathscr{L}$ is a linear self-adjoint differential operator of order $2p$ representing the system stiffness, ζ is a viscous damping operator, $m(P)$ is the system mass distribution, and $f(P,t)$ is the external force density. We concern ourselves with the case of light damping, for where the term $\zeta\dot{u}(P,t)$ is of at least one order of magnitude smaller than the remaining terms in Eq. (1). The associated boundary conditions are given by

$$B_i u(P,t) = 0,\ \ i = 1,2,...,p,\ \ p \in S \tag{2}$$

where B_i are linear differential operators of order 0 to $2p$ -1. The boundary conditions can either be geometric, in which case the order of B_i is no greater than p , or natural, in which case the order of B_i is greater than p. Functions satisfying the geometric boundary conditions are called admissible functions whereas functions satisfying all the boundary conditions are called comparison functions.

For the case of free vibration, consider the eigenvalue problem associated with Eq. (1)

$$\mathcal{L}\phi_r(P) = \lambda_r m(P)\phi_r(P), \quad r = 1,2,... \tag{3}$$

where $\phi_r(P)$ are functions that satisfy the boundary conditions

$$B_i\phi_r(P) = 0, i = 1,2,...,p, \quad r = 1,2,... \tag{4}$$

The solution to Eqs. (3) and (4) consists of a denumerably infinite set of real, non-negative eigenvalues λ_r and associated real eigenfunctions $\phi_r(P)$. The eigenvalues are related to the undamped natural frequencies of the system by $\lambda_r = \omega_r^2 (r = 1,2,...)$. For convenience, we order the eigenvalues so that $\lambda_1 \leq \lambda_2 \leq ...$.

The eigenfunctions obey the following orthonormality conditions:

$$\int_D m(P)\phi_r(P)\phi_s(P)dD = \delta_{rs}, \quad r,s = 1,2,... \tag{5}$$

and

$$\int_D \phi_r(P)\mathcal{L}\phi_s(P)dD = \lambda_r\delta_{rs}, \quad r,s = 1,2,... \tag{6}$$

where δ_{rs} is the Kronecker delta function. From the expansion theorem [25], we can express the displacement as

$$u(P,t) = \sum_{r=1}^{\infty} \phi_r(P) u_r(t) \tag{7}$$

where $u_r(t)$ are generalized coordinates and are modal coordinates for the undamped structure. Substituting Eq. (7) into Eq. (1), multiplying the result by $\phi_r(P)$, and integrating over the domain gives

$$\ddot{u}_r(t) + \sum_{r=1}^{\infty} c_{rs}\dot{u}_r(t) + \omega_r^2 u_r(t) = f_r(t), \quad r,s = 1,2,... \tag{8}$$

where

$$c_{rs} = \int_D \phi_r(P)\zeta\phi_s(P)dD, \quad r,s = 1,2,... \tag{9}$$

are small viscous damping coefficients and

$$f_r(t) = \int_D \phi_r(P)f(P,t)dD, \quad r = 1,2,... \tag{10}$$

are modal control forces.

Equations (8) represent an infinite set of ordinary differential equations that govern the response of lightly-damped, nearly self-adjoint distributed structures. The presence of high damping tends to destroy the decoupling nature, and the structure can no longer be classified as nearly self-adjoint. In the case of light levels of damping, however, the

self-adjointness property is preserved, and the generalized coordinates can be regarded as modal coordinates.

3.2 Correlation of the Modes of Vibration

Consider the case where the distributed structure is lightly-damped so that the system can be considered self-adjoint, which implies that the modes of vibration are spatially orthogonal and that the modes of vibration are uncorrelated in time [22]. In particular, the correlation condition between modal coordinates is given by

$$< \frac{d^n u_r(t)}{dt^n}, \frac{d^n u_s(t - T_o)}{dt^n} > = \frac{1}{\alpha_r} (\alpha_r + \omega_r)^{2n} |A_r|^2 e^{\alpha_r T_o} \cos \omega_r T_o \delta_{rs} \tag{11}$$

where α_r is the r^{th} modal decay rate, ω_r is the r^{th} natural frequency of oscillation, A_r is the r^{th} modal amplitude, and T_o is a time offset. Recall that $u_r(t)$ is the r^{th} modal coordinate. Also, the temporal inner product $< , >$ between any two generalized coordinates $q_r(t)$ and $q_s(t)$ is given by [25]

$$< q_r(t), q_s(t) > = \lim_{T \to \infty} \frac{1}{T} \int_0^T q_r(t) q_s(t) dt \tag{12}$$

Note from Eq. (11) that the temporal correlation of different modes is identically zero. Hence, the modes of vibration are uncorrelated in time.

3.3 Discretization

In general, closed-form solutions to Eq. (1) do not exist, so that we must consider an approximate solution. Commonly used techniques for obtaining approximate solutions are discretization techniques such as the finite element, the Rayleigh-Ritz, and the Galerkin methods. The techniques approximate the pde given by Eq. (1) by expressing the solution as a discrete linear combination of test functions multiplied by generalized coordinates. The Galerkin method is applicable to non-self-adjoint systems, in which the test functions must satisfy all the boundary conditions [25]. The finite element and Rayleigh-Ritz methods are applicable to self-adjoint systems, where the former can be regarded as a variant of the latter. The finite element and Rayleigh-Ritz methods are based on a variational principle, in which test functions need only be admissible functions and guarantee convergence to the exact solution of the pde [25].

Consider the admissible functions $\psi_r(P)$ (r = 1,2,...,n) and express the displacement $u(P,t)$ as a linear combination of the functions $\psi_r(P)$ multiplied by time-dependent generalized coordinates $q_r(t)$ as follows:

$$u^{(n)}(P,t) = \sum_{r=1}^{n} \psi_r(P) q_r(t) = \underset{\sim}{\Psi}^T(P) \underset{\sim}{q}_n(t) \tag{13}$$

where $u^{(n)}(P,t)$ is the n^{th} -order approximation of $u(P,t)$, $\underset{\sim}{\Psi}(P) = [\psi_1(P)...\psi_n(P)]^T$ is an n-vector of admissible functions, and $\underset{\sim}{q}_n(t)$ is an n-vector of generalized coordinates. The n-degree- of-freedom discretized model can be obtained using the finite series expansion given by Eq. (13) and has the form [25]

$$M^{(n)} \underset{\sim}{\ddot{q}}_n(t) + C^{(n)} \underset{\sim}{\dot{q}}_n(t) + K^{(n)} \underset{\sim}{q}_n(t) = \underset{\sim}{F}^{(n)}(t) \tag{14}$$

where

$$M^{(n)} = \int_D m(P)\underset{\sim}{\Psi}(P)\underset{\sim}{\Psi}^T(P)dD \tag{15a}$$

$$C^{(n)} = \int_D \underset{\sim}{\Psi}(P)[\zeta\underset{\sim}{\Psi}(P)]^T dD \tag{15b}$$

$$K^{(n)} = [\underset{\sim}{\Psi}(P), \underset{\sim}{\Psi}^T(P)] \tag{15c}$$

are n x n mass, damping, and stiffness matrices respectively, and

$$\underset{\sim}{F}^{(n)}(t) = \int_D \underset{\sim}{\Psi}(P)f(P,t)dD \tag{16}$$

is an n-dimensional generalized force vector. In addition, [,] is an energy inner product [25] obtained through integration by parts of $\int_D \underset{\sim}{\Psi}(P)(\mathscr{L}\underset{\sim}{\Psi}(P))^T dD$, and hence, is symmetric because $\mathscr{L}$ is self-adjoint. The energy inner product [u,u] is proportional to the potential energy of the system [25]. Since the structure is lightly-damped, the term $C^{(n)}\,\dot{\underset{\sim}{q}}_n(t)$ is of at least one order of magnitude smaller than the remaining terms in Eq. (14). We consider the undamped n-degree-of-freedom discrete model of the distributed structure. Unlike other discretization techniques, an attractive feature of the Rayleigh-Ritz method is that by increasing the number of degrees of freedom n , the previously calculated mass and stiffness coefficients do not change, so that one need only calculate an additional row (or column) to obtain the updated mass and stiffness matrices. For an (n+ 1)- degree-of-freedom discrete model, the mass and stiffness matrices have the form

$$M^{(n+1)} = \begin{bmatrix} & & x \\ & M^{(n)} & x \\ x & x & x \end{bmatrix}, \quad K^{(n+1)} = \begin{bmatrix} & & x \\ & K^{(n)} & x \\ x & x & x \end{bmatrix} \tag{17}$$

The eigenvalue problems associated with the discrete models are given by

$$\lambda_r^{(n)} M^{(n)} \underset{\sim}{x}_r^{(n)} = K^{(n)} \underset{\sim}{x}_r^{(n)}, \quad r = 1,2,...,n \tag{18}$$

and

$$\lambda_r^{(n+1)} M^{(n+1)} \underset{\sim}{x}_r^{(n+1)} = K^{(n+1)} \underset{\sim}{x}_r^{(n+1)}, \quad r = 1,2,...,n+1 \tag{19}$$

The inclusion principle [25] requires the eigenvalues of the n-degree-of-freedom model and the eigenvalues of the (n+1)-degree-of-freedom model to obey the relationship

$$\lambda_1^{(n+1)} \leq \lambda_1^{(n)} \leq \lambda_2^{(n+1)} \leq \lambda_2^{(n)} \leq ... \leq \lambda_n^{(n)} \leq \lambda_{n+1}^{(n+1)} \tag{20}$$

As the number of degrees of freedom n in the discrete model is increased, the approximate eigenvalues decrease monotonically and approach the actual eigenvalues of the system asymptotically from above [25].

3.4 Modal Identification of Lightly-Damped Structures

We wish to use free response measurements to obtain estimates of the system's natural frequencies and mode shapes. Due to the discretization procedure, only approximations to the modes of vibration can be obtained. It will be shown that the identified

eigenvalues obey the inclusion principle as was the case for the Rayleigh-Ritz method so that the identified eigenvalues approach the system eigenvalues monotonically from above as the order of the model is increased. Consider correlating the derivatives of the generalized coordinates $\underset{\sim}{q}_n(t)$ and define

$$A^{(n)} = < \frac{d^m}{dt^m} \underset{\sim}{q}_n(t), \ \frac{d^m}{dt^m} \underset{\sim}{q}_n^T(t) > \tag{21}$$

and

$$B^{(n)} = < \frac{d^k}{dt^k} \underset{\sim}{q}_n(t), \ \frac{d^k}{dt^k} \underset{\sim}{q}_n^T(t - T_o) > \tag{22}$$

The generalized coordinates can be written as a linear combination of the eigenvectors $\underset{\sim}{x}_r$ (r = 1,2,...,n) multiplied by the modal coordinates, or

$$\underset{\sim}{q}_n(t) = \sum_{r=1}^{n} \underset{\sim}{x}_r^{(n)} u_r(t) \tag{23}$$

Substituting Eq. (23) into Eqs. (21) and (22), we arrive at

$$A^{(n)} = \sum_{r=1}^{n} \sum_{s=1}^{n} \underset{\sim}{x}_r^{(n)} \underset{\sim}{x}_s^{(n)T} < \frac{d^m u_r(t)}{dt^m}, \ \frac{d^m u_s(t)}{dt^m} > \tag{24}$$

and

$$B^{(n)} = \sum_{r=1}^{n} \sum_{s=1}^{n} \underset{\sim}{x}_r^{(n)} \underset{\sim}{x}_s^{(n)T} < \frac{d^k u_r(t)}{dt^k}, \frac{d^k u_s(t - T_o)}{dt^k} > \tag{25}$$

Now consider the algebraic eigenvalue problem

$$\lambda_r^{(n)} A^{(n)} \underset{\sim}{v}_r^{(n)} = B^{(n)} \underset{\sim}{v}_r^{(n)} \tag{26}$$

By using Eq. (11) in Eqs. (24) and (25) and substituting the result into Eq. (26) gives

$$\lambda_r^{(n)} \sum_{s=1}^{n} \frac{1}{\alpha_s} (\alpha_s + \omega_s)^{2m} |A_s|^2 \underset{\sim}{x}_s^{(n)} \underset{\sim}{x}_s^{(n)T} \underset{\sim}{v}_r^{(n)} = \tag{27}$$

$$\sum_{s=1}^{n} \frac{1}{\alpha_s} (\alpha_s + \omega_s)^{2k} |A_s|^2 \underset{\sim}{x}_s^{(n)} \underset{\sim}{x}_s^{(n)T} e^{\alpha_s T_o} \cos \omega_s T_o \underset{\sim}{v}_r^{(n)}$$

It can be shown by using the orthonormality conditions, Eq. (18), that the solution to Eq. (27) is given by

$$\underset{\sim}{v}_r^{(n)} = M^{(n)} \underset{\sim}{x}_r^{(n)} \tag{28}$$

and

$$\lambda_r^{(n)} = (\alpha_r + \omega_r)^{2(k-m)} e^{\alpha_r T_o} \cos \omega_r T_o \tag{29}$$

The TCM for modal identification proceeds as follows: First, the matrices $A^{(n)}$ and $B^{(n)}$ are computed by correlating the generalized coordinates $\underset{\sim}{q}_n(t)$. In practice the general-

ized coordinates can be replaced by actual sensor measurements, i.e., accelerations, velocities, angular rates, etc.. Then, the eigenvalue problem of Eq. (26) is solved to obtain $\lambda_r^{(n)}$ and $\underset{\sim}{y}_r^{(n)}$. Finally, Eqs. (28) and (29) provide the relationship between the eigenvalues and eigenvectors of Eq. (26) to the identified natural frequencies and mode shapes of the system.

Consider the case where we let $k = m$ in Eqs. (21) and (22). With the light damping restriction ($\alpha_r << 1$), we obtain

$$\omega_r = \frac{1}{T_o} \cos^{-1} \lambda_r^{(n)} \tag{30}$$

Now consider the case where we let $k = 2$, $m = 1$, and $T_o = 0$. This gives us

$$\omega_r = \sqrt{\lambda_r} \tag{31}$$

The first case suggests that we use the same type of sensor measurement in computing both $A^{(n)}$ and $B^{(n)}$, the only difference being the time offset T_o. In the second case, we use velocities for the correlation in Eq. (21) and accelerations in Eq. (22) and the time offset is identically zero.

In practice the temporal correlations must be truncated in finite time. If the integration is not carried out far enough, the results will not be accurate. In general, it is necessary for the total integration time to be at least six times the fundamental period or $T_\infty \geq 12\pi/\omega_1$. An additional restriction must be placed on the sampling interval such that $T_s \leq \pi/5\omega_n$. These requirements on the integration time and sampling interval are not clear cut. They are only given here as a guideline, and experimentation should be performed to determine if they have been met for a particular case.

In summary, the sensor measurements are correlated to obtain two n x n matrices $A^{(n)}$ and $B^{(n)}$. An eigenvalue problem is solved involving these two matrices, and the

eigenvalues and eigenvectors are directly related to the identified natural frequencies and mode shapes of the system. Because of the way in which $A^{(n)}$ and $B^{(n)}$ are computed, the eigenvalues of Eq. (26) obey the inclusion principle. Specifically, since the higher order models have similar structure to Eq. (17) in that they are formed by adding rows and columns to the existing $A^{(n)}$ and $B^{(n)}$, the (n+1)-degree-of-freedom model eigenvalues obey Eq. (20).

4 The Eigensystem Realization Algorithm

4.1 Equations of Motion

For the Eigensystem Realization Algorithm, we consider the state space model of a finite dimensional, discrete-time, linear, time-invariant dynamical system given by

$$\underset{\sim}{x}(k+1) = \Phi \underset{\sim}{x}(k) + \Gamma \underset{\sim}{u}(k) \tag{32}$$

and

$$\underset{\sim}{y}(k) = H \underset{\sim}{x}(k) \tag{33}$$

where $\underset{\sim}{x}$ is an n-dimensional state vector, $\underset{\sim}{u}$ is an m-dimensional input vector, and $\underset{\sim}{y}$ is a p-dimensional output vector. The dynamical properties of the system are contained within the matrix Φ. Our goal is to extract the modal parameters from the free or impulse response measurements. A realization is obtained by finding matrices

[Φ, Γ, H] that satisfy Eqs. (32) and (33) so that the outputs of the discrete model match those of the actual system while considering the noise in the sensor measurements.

4.2 The Hankel Matrix

The foundation of the ERA is in the formation of the generalized Hankel matrix. It is composed of impulse or free response sensor measurements. The Hankel matrix is actually an r x s block matrix with each block having dimension l x m where l is the number of sensors used in the analysis and m is the number of response sets used. The use of multiple response records is particularly useful in identifying repeated eigenvalues. The overall dimension of the generalized Hankel matrix is (lr) x (ms) and has the form

$$H(k-1) = \begin{bmatrix} Y(k) & Y(k+1) & \bullet\ \bullet\ \bullet & Y(k+s-1) \\ Y(k+1) & Y(k+2) & & \\ \bullet & & \bullet & \\ \bullet & & & \bullet \\ \bullet & & & \\ Y(k+r-1) & & & Y(k+s+r-2) \end{bmatrix} \tag{34}$$

The more general form of the algorithm allows for arbitrary integer increments in the Hankel matrix [7] opposed to the unity increments considered here.

4.3 The Singular Value Decomposition

The ERA uses the singular values of H(0) to obtain a minimum-order realization. In this section we show a method for obtaining the singular values of a rectangular matrix that uniquely defines its singular value decomposition (SVD). Consider the decomposition of $H(0)$ and $H^T(0)$

$$H(0) = USV^T \tag{35}$$

and

$$H^T(0) = VS^TU^T \tag{36}$$

where the (lr) x (lr) matrix U and the (ms) x (ms) matrix V are isometric so that $UU^T = I$ and $VV^T = I$. Also note that S is diagonal and has dimension (lr) x (ms), the same dimension as $H(0)$. Now we can form

$$H^T(0)H(0)V = VS^2 \tag{37}$$

and

$$H(0)H^T(0)U = US^2 \tag{38}$$

where S^2 is a square diagonal matrix. Consider the two eigenvalue problems

$$G\underline{v}_i = \underline{v}_i\lambda_i \tag{39}$$

and

$$G^T\underline{u}_i = \underline{u}_i\lambda_i \tag{40}$$

where $G = H^T(0)H(0)$. Note that the eigenvalues of Eqs.(39) and (40) are simply the squares of the singular values of $H(0)$. Also, the eigenvectors $\underline{v}_i$ and $\underline{u}_i$ are the columns of the matrices V and U respectively.

Therefore, the singular values of H(0) can be found from the eigenvalues of $H^T(0)H(0)$. In addition, the eigenvectors of $H^T(0)H(0)$ and $H(0)H^T(0)$ provide the columns of V and U, respectively. In general, however, the solutions to Eqs. (37) and (38) are not recommended for the SVD as the matrix G in Eqs. (39) and (40) is more ill-conditioned when compared to the matrix $H(0)$.

4.4 Minimum Order Realization

The matrices U, S, and V can be partitioned such that $H(0) = PDQ^T$ where P has dimension (lr) x n, D has dimension n x n, and Q has dimension (ms) x n. The matrices P, D, and Q are further partitioned by retaining only the singular values pertaining to the system modes. Using this partitioned decomposition, it can be shown [7] through a series of matrix manipulations that the minimum order realization, i.e., the triple $[\Phi, \Gamma, H]$, is given by

$$[\Phi, \Gamma, H] = [D^{-1/2}P^TH(1)QD^{-1/2}, D^{1/2}Q^TE_m, E_p^TPD^{1/2}] \tag{41}$$

where $E_m^T = [I_m, 0_m, ..., 0_m]$ is an m x (ms) matrix and $E_p^T = [I_p, 0_p, ..., 0_p]$ is an l x (lr) matrix.

4.5 Modal Parameter Identification

As was mentioned before, the generalized Hankel matrix has dimension (lr) x (ms). The number of singular values will be equal to the greater of the row and column dimension. For n modes participating in the system response, all but $2n$ of these singular values will be zero for the case of no noise in the output measurements. Since in practical applications there is always some noise present, these singular values are not zero but are relatively small. Also in practice we do not know how many modes are participating in the response. Therefore, the procedure is to place the singular values in descending order, establish a criterion for determining the minimum-order $2n$, of the identified system, and partition P, D, and Q [7].

The next step in the process is to solve the eigenvalue problem

$$\Phi\psi_r = \psi_r z_r, \quad r = 1,2,...,2n \tag{42}$$

where Φ is the realized transition matrix given by

$$\Phi = D^{-1/2} P^T H(1) Q D^{-1/2} \tag{43}$$

The identified eigenvalues obtained from the solution of Eq. (42) are in the z-plane, as the original formulation was in discrete time. The eigenvalues can be transformed to the s-plane using the relationship

$$s_r = \frac{(\ln z_r \pm i2j\pi)}{\Delta\tau} \tag{44}$$

where j is an integer usually taken to be zero and $\Delta\tau$ is the sampling interval. In general the identified eigenvalues are complex in which the real parts represent the identified

modal damping rates and the imaginary parts represent the identified damped natural frequencies of the structure. For light levels of damping, it is usually sufficient to take the imaginary parts as being the identified natural frequencies of the system. The mode shapes are contained in the matrix

$$\mathbf{M} = E_p^T P D^{1/2} \psi \tag{45}$$

where M is called the identified eigenvector matrix or the identified modal participation matrix.

In real applications the number of modes participating in the response is not known a priori and measurement noise degrades the results of the identification in which "noise modes" are identified. An accuracy indicator used to quantify the degree to which a particular mode is likely to be a system mode was developed by Juang and Pappa [7]. The indicator determines the coherence between the predicted modal amplitude history using the actual data and an ideal one based on the identified eigenvalue and eigenvector of each identified mode. The coherence is appropriately named the modal amplitude coherence.

We can summarize the procedure for modal identification in the ERA as follows: (1) construct the generalized Hankel matrix from the free response data, (2) perform the singular value decomposition as given by Eq. (35) and obtain the matrices P, D, and Q through partitioning, (3) inspect the singular values and determine the minimum-order of the system, (4) partition P, D, and Q further based on the minimum-order, (5) identify the eigenvalues and mode shapes by solving the eigenvalue problem of Eq. (42), and (6) calculate the modal amplitude coherence for each identified mode.

5 TCM: A Constrained Version of the ERA

5.1 Introduction

It was discovered that the TCM is a constrained version of the ERA (CERA) for lightly-damped structures. This result has important implications. By constraining the ERA, the modal identification may be less sensitive to sensor noise [24]. Furthermore, the modal identification for the ERA requires the solution of a $2n$ x $2n$ algebraic eigenvalue problem, where n is the number of identified modes. On the other hand, the CERA requires the solution of an n x n algebraic eigenvalue problem, as the modal identification is performed in the configuration space. Moreover, the eigenvalues and eigenvectors obtained from the modal identification are complex for the ERA while they are real for the CERA. The eigenvectors for the CERA are orthogonal as well.

The constraint used is to require the generalized Hankel matrix to have only one row of block matrices. For n modes identified, we must have $l \geq n$, where l is the number of sensors used in the analysis. The method can use multiple data sets, as was the case

for the ERA, to identify repeated or closely-space frequencies [24]. In the development given here, we consider only a single data set.

5.2 Theoretical Development

Consider a constrained generalized Hankel matrix, $H_c(k)$, which has only a single row of block matrices. The constrained Hankel matrix has dimension l x s, where we have taken $m = 1$, although this is not a constraint for the CERA. The matrices $A^{(n)}$ and $B^{(n)}$ in Eqs. (21) and (22) can be written as

$$A^{(n)} = \frac{1}{s} H_c(k) H_c^T(k) \tag{46}$$

and

$$B^{(n)} = \frac{1}{s} H_c(k+1) H_c^T(k) \tag{47}$$

in which the derivatives in the two inner products are of the same order, and the time offset, T_o, is equal to the sampling interval. Note that the column dimension of the Hankel matrix must be large enough to sufficiently correlate the sensor measurements as is required by the TCM.

Equations (46) and (47) express the correlation matrices used in the TCM in terms of the generalized Hankel matrix used in the ERA. This is the fundamental step in the development of the CERA. Substituting Eqs. (46) and (47) into the eigenvalue problem of Eq. (26) gives

$$\lambda_r H_c(k) H_c^T(k) \underline{v}_r = H_c(k+1) H_c^T(k) \underline{v}_r \tag{48}$$

where the superscripts have been dropped for convenience.

Using the singular value decomposition of $H_c(k)$, Eq. (48) becomes

$$\lambda_r P D Q^T Q D^T P^T \underline{v}_r = H_c(k+1) Q D^T P^T \underline{v}_r \tag{49}$$

where D is an n x n diagonal matrix, P is an l x n matrix, and Q is an s x n matrix. By making use of the orthonormality properties of P and Q, we have

$$\lambda_r P D^2 P^T \underline{v}_r = H_c(k+1) Q D P^T \underline{v}_r \tag{50}$$

With the definition $\underline{w}_i = D P^T \underline{v}_i$, Eq. (50) can be written as

$$\lambda_r P D^{1/2} \underline{w}_r = H_c(k+1) Q D^{-1/2} \underline{w}_r \tag{51}$$

Premultiplying Eq.(51) by $D^{-1/2} P^T$ gives us

$$\lambda_r \underline{w}_r = D^{-1/2} P^T H_c(k+1) Q D^{-1/2} \underline{w}_r \tag{52}$$

Comparing Eq. (52) to the eigenvalue problem we encountered in the ERA formulation, Eqs. (42) and (43), we see that they are identical except for two important aspects. In the ERA formulation the order of the eigenvalue problem is $2n$, while Eq. (52) represents an eigenvalue problem of order n. Hence, for cases of light damping, the TCM reduces to a constrained version of the ERA. Furthermore, the relationship between the eigenvalues of Eq. (52) and the identified natural frequencies is provided by Eq. (30) instead of Eq. (44).

The procedure in the CERA is the same as that proposed by the ERA, with the following exceptions: (1) the Hankel matrix is composed of only one row of block ma-

trices; (2) only n singular values are retained in the system realization; (3) an n x n algebraic eigenvalue problem is solved opposed to the $2n$ x $2n$ algebraic eigenvalue problem required by the ERA; and (4) the modal identification is performed using Eq. (30) instead of Eq. (44). Numerical examples will be provided in chapter six to demonstrate the procedure and to examine the accuracy of the method.

Like the ERA, the CERA identifies natural frequencies and mode shapes for lightly-damped systems. The CERA does not identify modal damping directly as in the ERA. Damping tends to be more sensitive to sensor measurement noise so that, in practice, it is quite difficult to obtain accurate estimates of the damping. Recent developments, however, show that the CERA in conjunction with modal filters does provide improved damping estimates [24].

6 Simulation Results

6.1 Demonstration of the TCM and the ERA

In this section we provide several cases to illustrate the TCM and the ERA. We consider cases in which there is (1) no damping in the system and no noise in the sensor measurements, (2) damping without noise, (3) noise without damping, and (4) damping with noise. For all four cases we simulate the response of a simply supported beam subjected to an impulse force at $x = 2L/7$ with the six lowest modes participating in the response. The beam has uniform properties with length $L = 5m$, bending rigidity $EI = 30Nm$, and mass density $m = 1kg/m$. With these values, the eigenvalue problem of Eq. (3) has the closed-formed solution [25] $\omega_r = \sqrt{30}\,(\frac{r\pi}{5})^2\,(r = 1,2,...)$ and $\phi_r(x) = \sqrt{\frac{2}{5}}\,\sin(\frac{r\pi x}{5})\,(r = 1,2,...)$. For each case, six acceleration sensors were used at positions $x_i = \frac{iL}{7}$. Also, for the TCM, we use velocities in the correlation of Eq. (21) and accelerations in the correlation of Eq. (22), so that the identified eigenvalues and eigenvectors are obtained from Eqs. (26), (28), and (31). The size of the Hankel matrix for the ERA is defined by the parameters $r = 24$, $l = 6$, $s = 100$, and $m = 1$ in Eq.

(34). In addition, the temporal inner products for the TCM are truncated after 29 sec., or ten times the fundamental period. The sampling time is taken to be one-tenth of the shortest period.

The first three identified natural frequencies for case (1) are illustrated in Table 1. Both methods give good results for no damping and no noise, however the ERA identifies the natural frequencies exactly, while for the TCM there is a small error. This is attributed to the truncation of the temporal inner products given by Eqs. (21) and (22). The identified mode shapes for the TCM and the ERA are also consistent with the first three mode shapes of a simply supported beam as shown in Figs. 1 and 2.

Table 1. Identified frequencies with $\zeta = 0, \eta = 0\%$

r =	ω_r-TCM	ω_r-ERA	ω_r -actual
1	2.1659	2.1623	2.1623
2	8.6617	8.6493	8.6493
3	19.474	19.461	19.461

Now we look at the case where we include damping in the response. Of course, in real applications there is always some level of damping present. Here we consider a damping coefficient of $\zeta = .05$. This is consistent with the light damping restriction

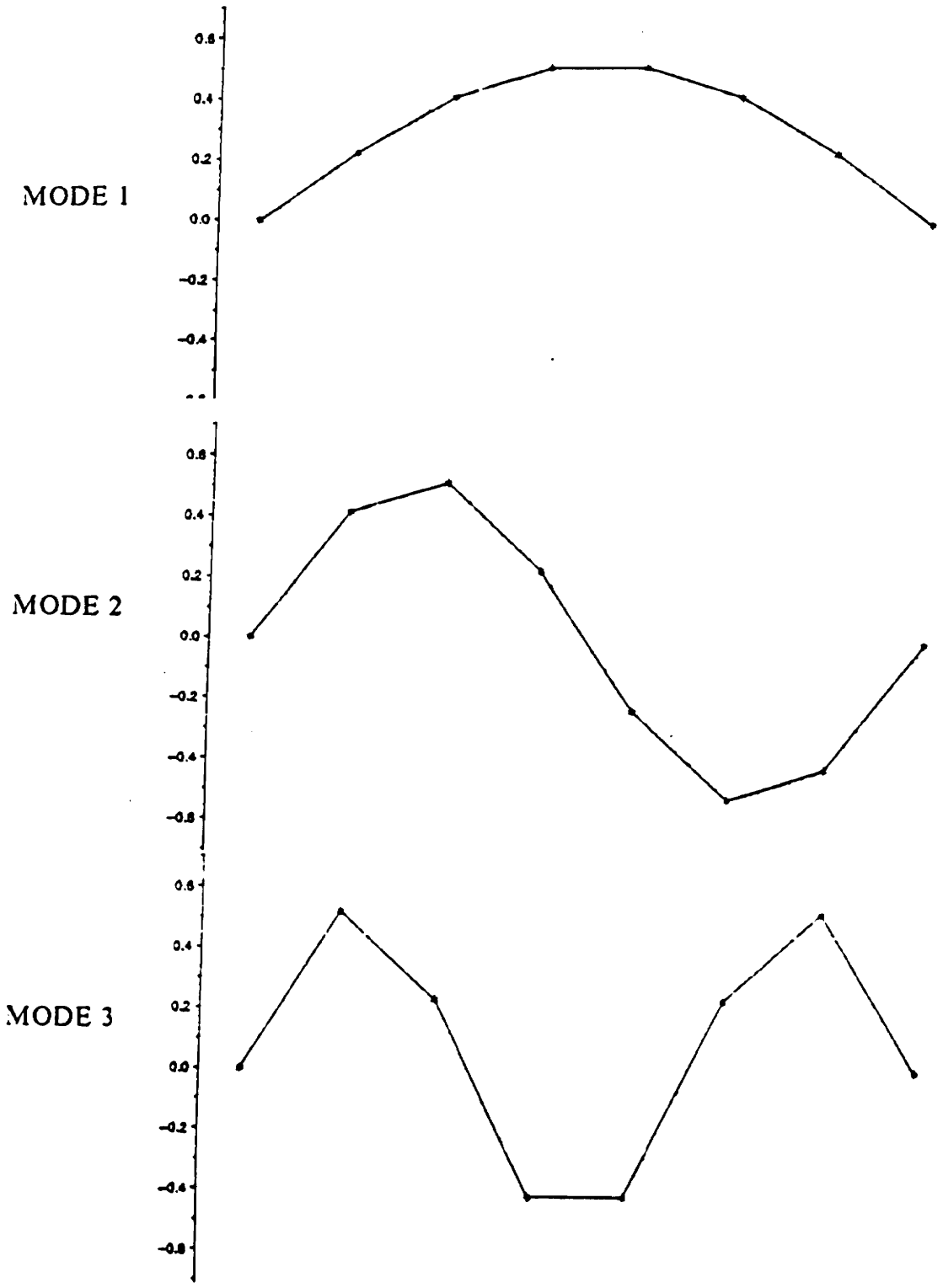

Figure 1. Identified mode shapes of a simply supported beam using the TCM with $\zeta = 0$, $\eta = 0\%$

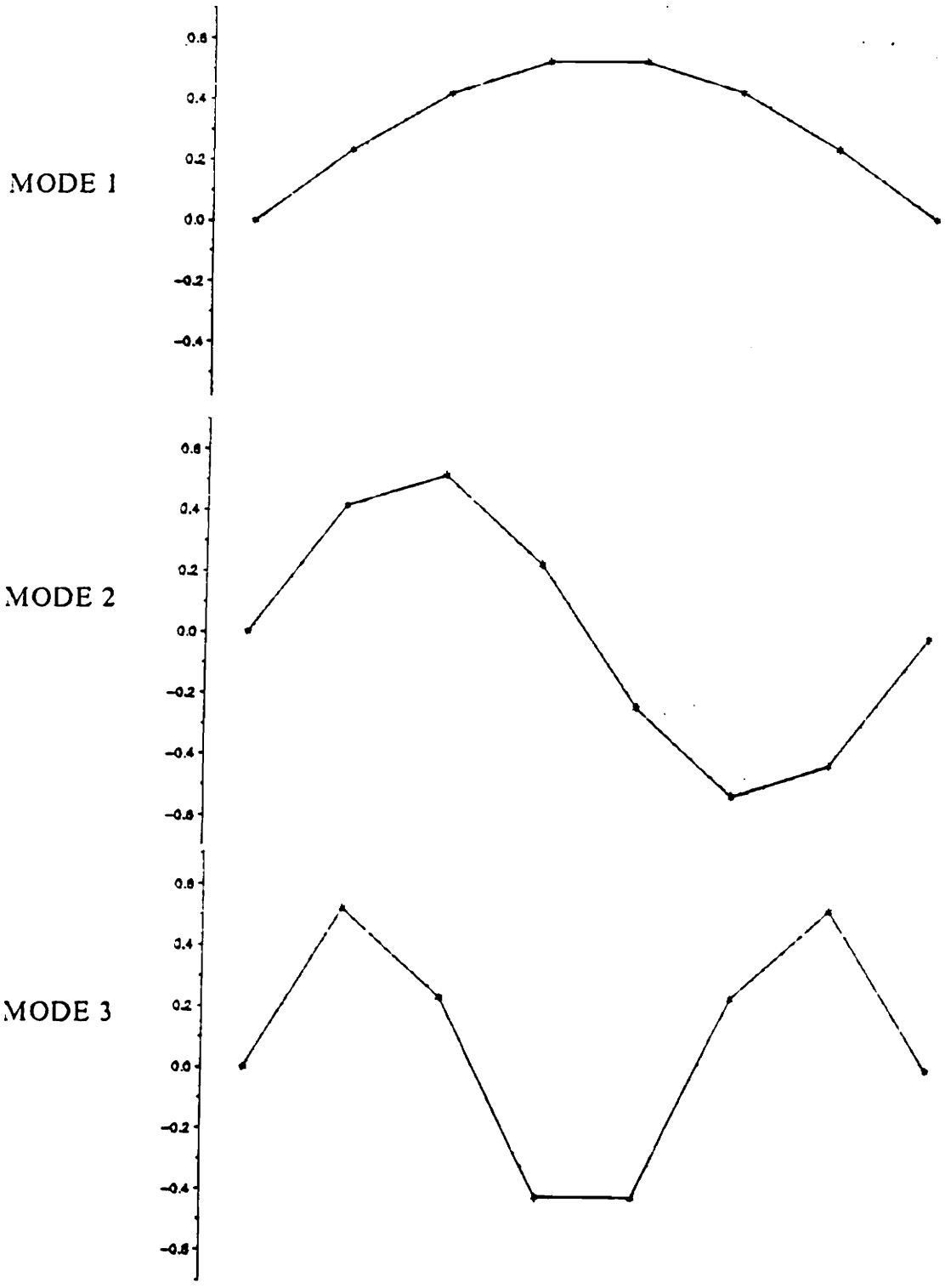

Figure 2. Identified mode shapes of a simply supported beam using the ERA with $\zeta = 0$, $\eta = 0\%$

imposed by the TCM, and it is representative of many real systems. The first three identified natural frequencies are shown in Table 2.

Table 2. Identified frequencies with ζ = .05, η = 0%

r =	ω_r-TCM	ω_r-ERA	ω_r-actual
1	2.1711	2.1623	2.1623
2	8.6614	8.6493	8.6493
3	19.407	19.461	19.461

Notice that the identified natural frequencies for both methods are still quite good for this case. It is interesting to note that each of the identified natural frequencies for the TCM are affected by different amounts by the damping with the largest deviation from the undamped case being .34% for mode 3. On the other hand, the identified frequencies obtained by the ERA do not change and still give exact results. The mode shapes for the ERA in the case of damping also do not change with respect to the undamped case. They are not affected by the addition of damping. Conversely, the mode shapes identified by the TCM do undergo some change from the undamped case. These changes caused by damping are slight, however, with the maximum error in any element of the three identified eigenvectors, when compared to case (1), being .12% for mode mode 1, .81% for mode 2, and 4.1% for mode 3. The mode shapes are shown in Figs. 3 and 4.

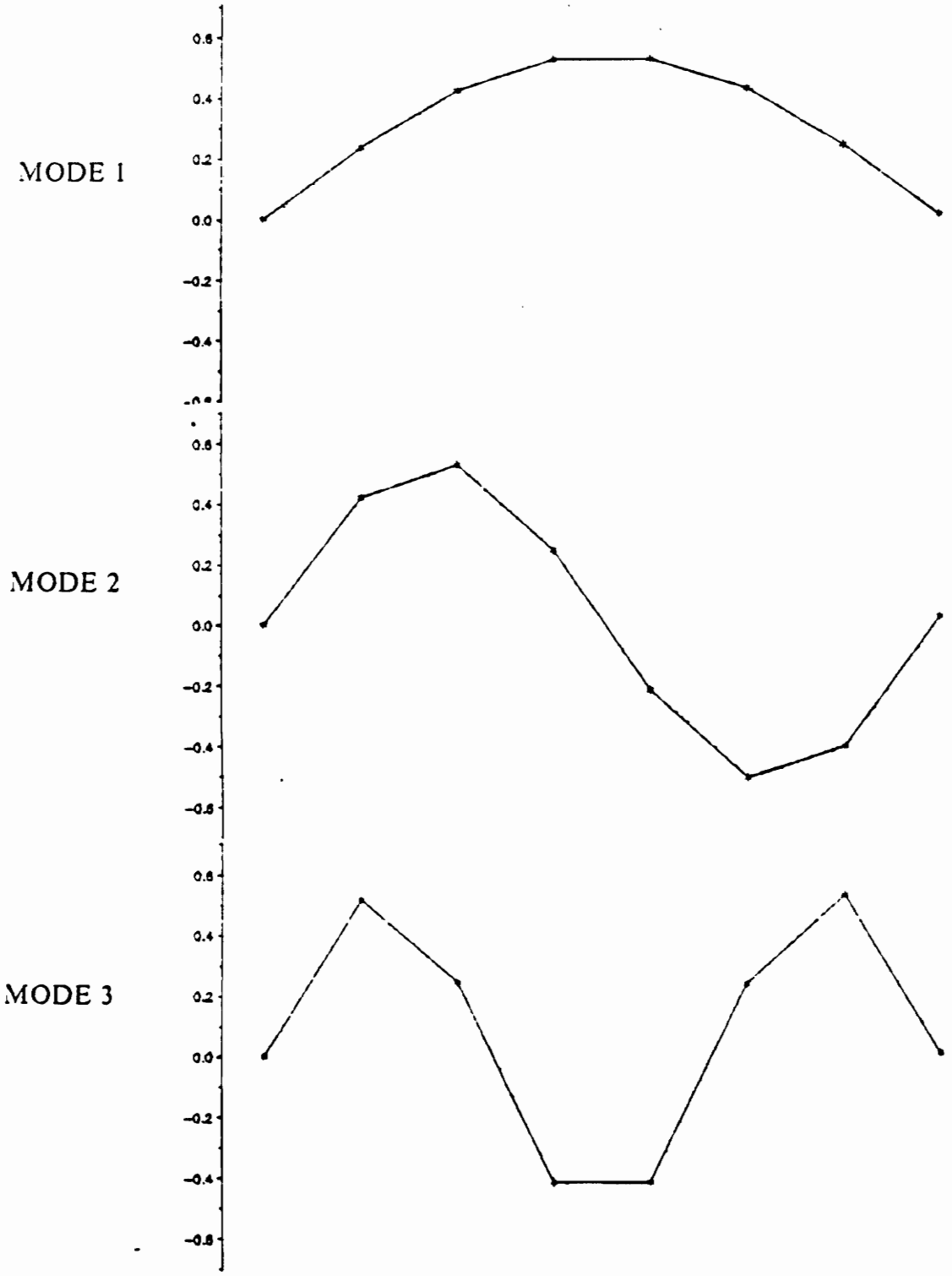

Figure 3. Identified mode shapes of a simply supported beam using the TCM with ζ = .05 , η = 0%

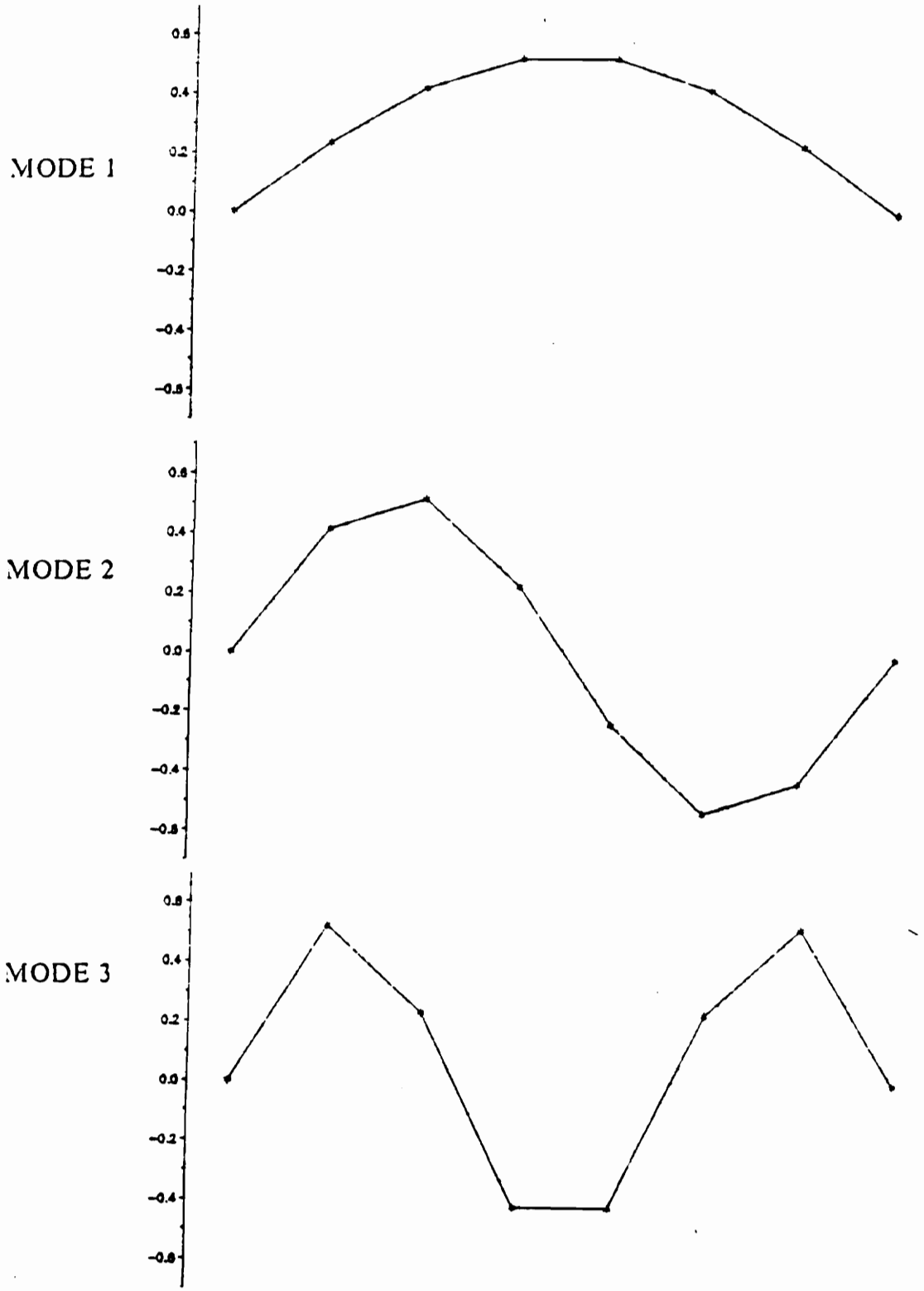

Figure 4. Identified mode shapes of a simply supported beam using the ERA with ζ = .05 , η = 0%

Next we consider the case where Gaussian noise is added to the sensor outputs such that at one standard deviation, the noise added is 5% of the measurement, which we denote by $\eta = 5\%$. In addition, there is no damping. The identified natural frequencies are given in Table 3. Notice that the TCM gives better results than does the ERA for the first two modes, but the ERA is better for the third mode. In other words, the lower modes for the TCM are less sensitive to noise than are the lower modes for the ERA, but for the higher modes we find the opposite effect. As for the identified eigenvectors, the TCM gives the better results, although the results for the ERA are still consistent with the actual eigenvectors of the system. For both methods the first identified eigenvector has the smallest deviation from case (1). However, the average deviation is 3.0% for the ERA and only 0.1% for the TCM. For the TCM the third mode had the largest deviation with an average of 4.0%, while for the ERA the second mode had the largest deviation with an average of 8.0%. The identified mode shapes are shown in Figs. 5 and 6.

Table 3. Identified frequencies with $\zeta = 0$, $\eta = 5\%$

r =	ω_r-TCM	ω_r-ERA	ω_r-actual
1	2.1706	2.1033	2.1623
2	8.6469	8.7314	8.6493
3	18.499	19.469	19.461

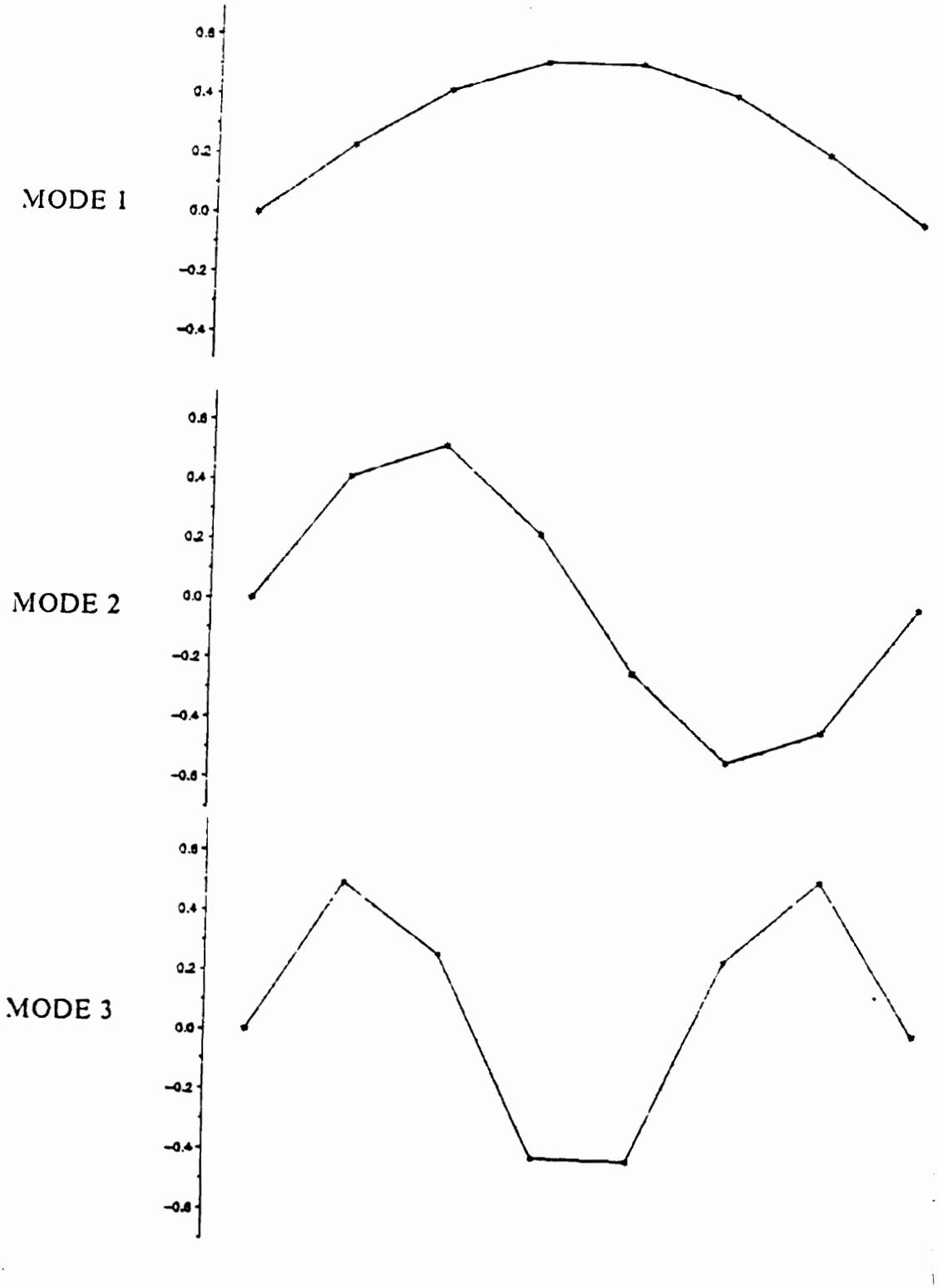

Figure 5. Identified mode shapes of a simply supported beam using the TCM with $\zeta = 0$, $\eta = 5\%$

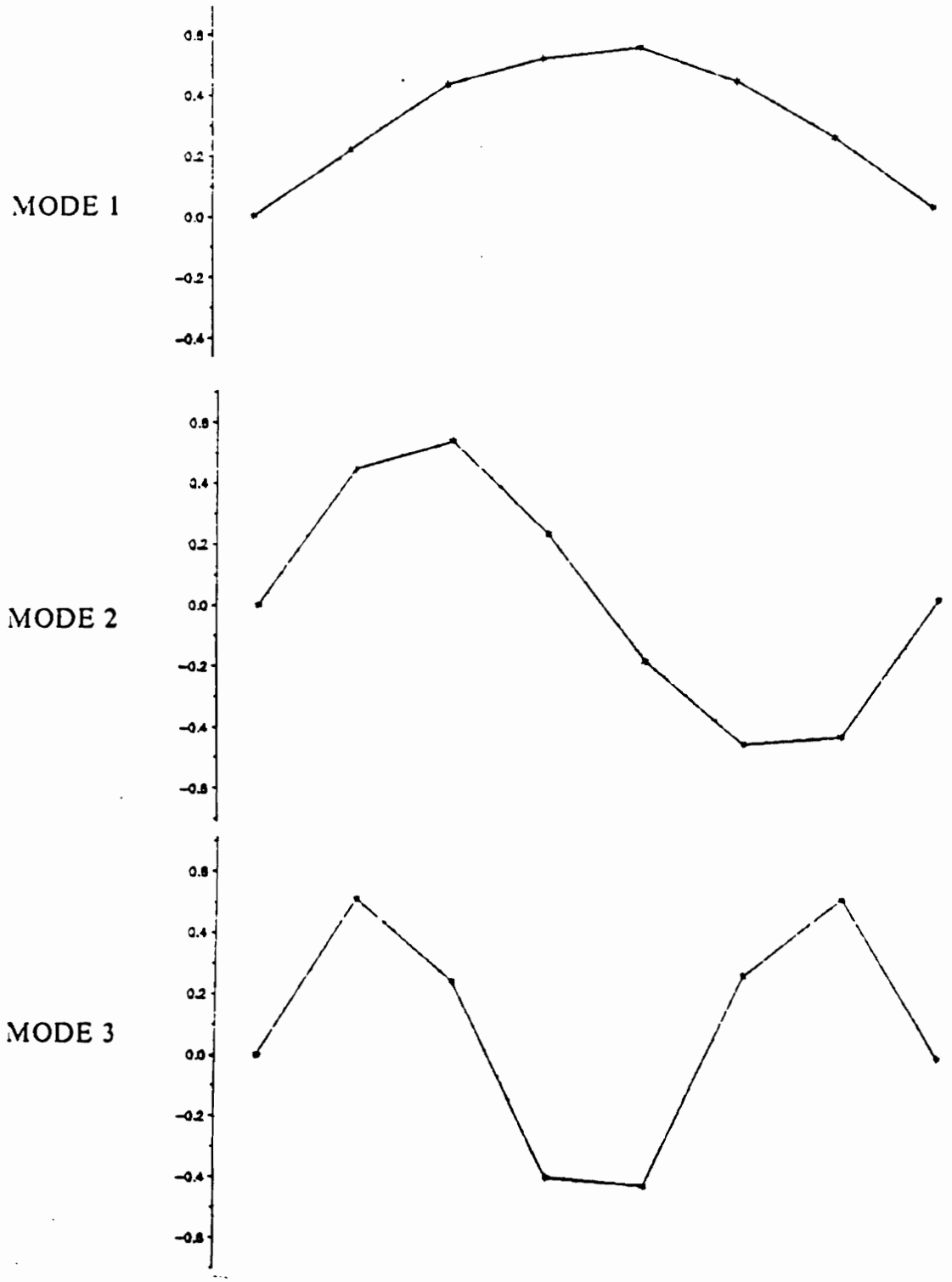

Figure 6. Identified mode shapes of a simply supported beam using the ERA with ζ = 0 , η = 5%

Finally, we include both damping and noise with values $\zeta = .01$ and $\eta = 3\%$. Table 4 contains the identified natural frequencies for the two methods. The TCM once again gives the more accurate estimates for the first two modes, however the ERA performs better than in case (3). This should be expected because the level of noise has been decreased. The second and third modes for the TCM are worse than in case (3) because of the addition of damping.

Table 4. Identified frequencies with $\zeta = .01$, $\eta = 3\%$

r =	ω_r-TCM	ω_r-ERA	ω_r-actual
1	2.1655	2.1579	2.1623
2	8.6192	8.6881	8.6493
3	17.140	19.455	19.461

The identified mode shapes for the two methods are shown in Figs.7 and 8. For this case, the TCM gives more accurate estimates for the first two modes, while the ERA is better for the third mode. This follows the pattern exhibited by the identified frequencies.

As a result of the following tests, we note the following: (1) the ERA provides exact results for cases with no noise, regardless of the damping, while the TCM incurs a small error from the truncation of the temporal inner products and from any damping; (2) the TCM, for some noise levels, is less sensitive to noise for the identifed lower frequencies;

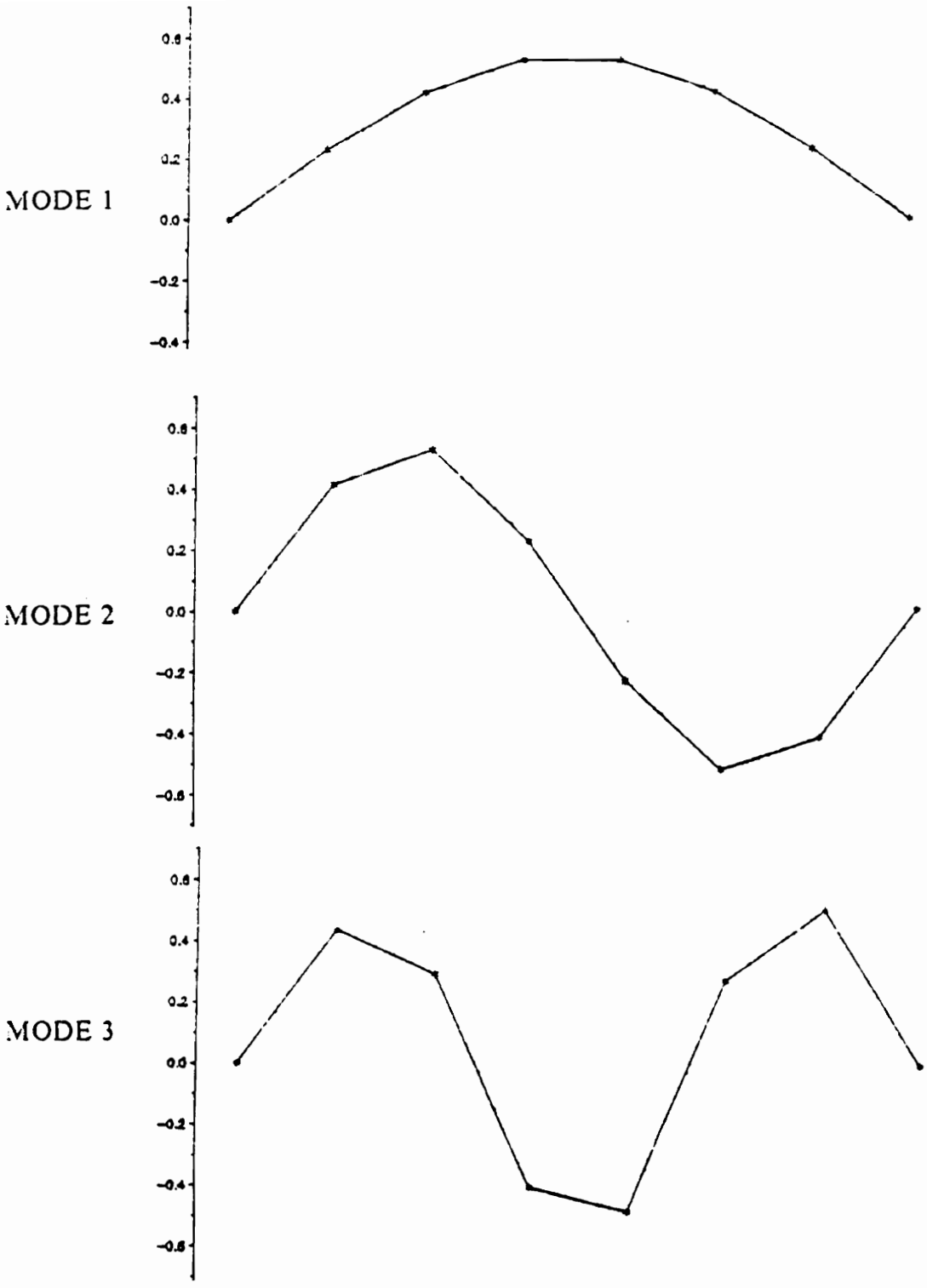

Figure 7. Identified mode shapes of a simply supported beam using the TCM with ζ = .01 , η = 3%

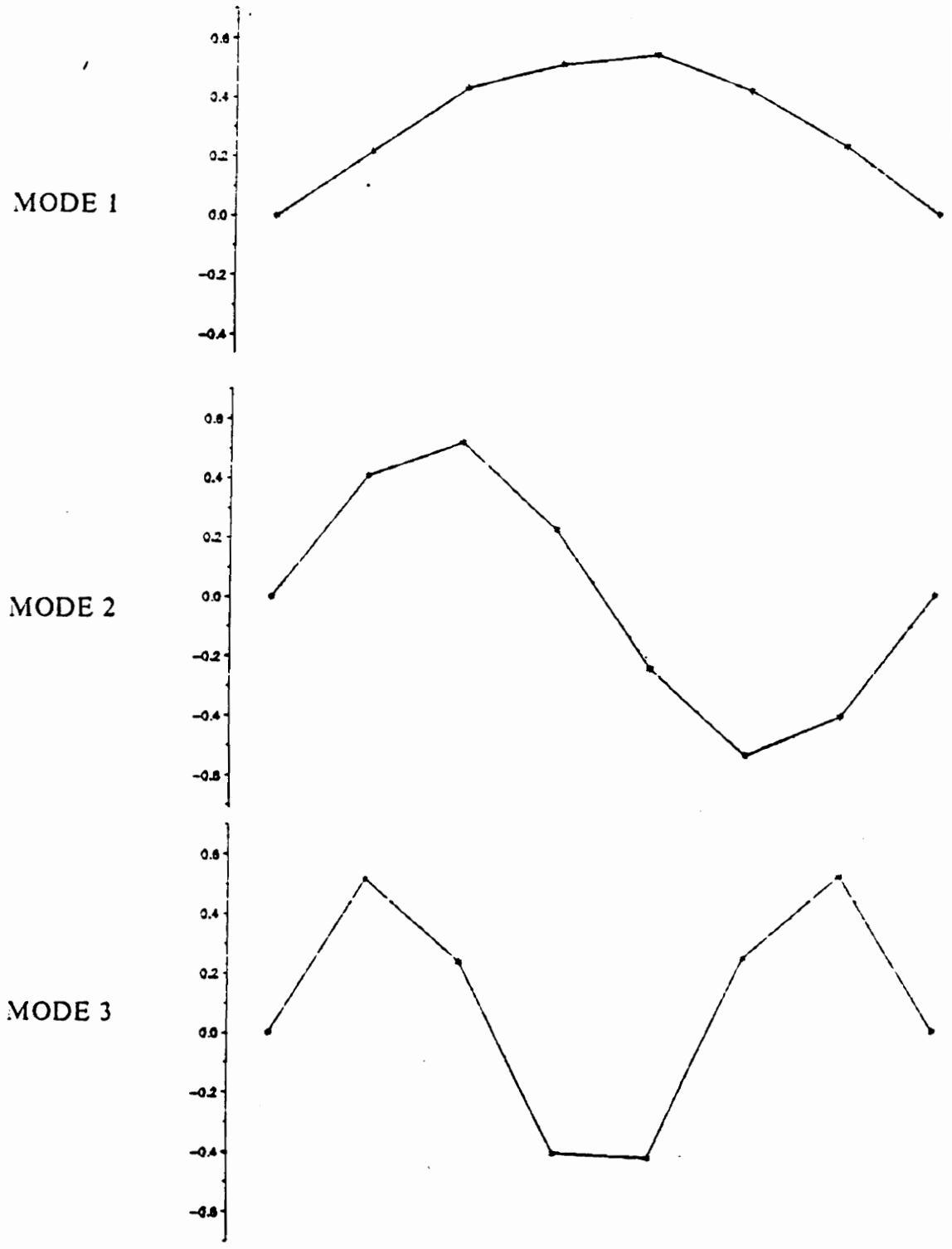

Figure 8. Identified mode shapes of a simply supported beam using the ERA with ζ = .01 , η = 3%

and (3) in the presence of noise, the identified mode shapes for the lower modes are much better for the TCM than for the ERA, but the ERA still gives reasonable results.

6.2 Comparison of Noise Effects

We wish to investigate the effect of adding noise to simulated data on the identified eigenvalues or natural frequencies for both the TCM and the ERA. In particular, we compare the performance of the two methods when the amount of noise added is increased. This type of study provides some insight into how to interpret identified results in actual applications in addition to determining if either method can be considered superior in dealing with noise.

Consider the simply supported beam of the previous section with both damping and noise simulated in the response. The value of damping is fixed at $\zeta = .01$, while the noise added takes on values from $\eta = 2.7\%$ to $\eta = 3.4\%$. As was the case previously, the beam is excited by an initial impulse at $x = 2L/7$. Plots of the signal-to-noise ratio (snr) versus the identified frequencies for the first three modes are shown in Figs. 9, 10, and 11 respectively. The solid lines represent the actual values.

As can be seen, the identified values tend to converge to the actual values as the *snr* approaches infinity. There are, however, differences in the rates of convergence. For example, the first identified frequency for the TCM exhibits little variation as the noise is decreased, while the first identified frequency for the ERA undergos considerable change. In addition, we notice that as the noise decreases past a certain value, the first identified frequency for the ERA becomes better than its TCM counterpart. For the second mode, the rates of convergence are similar, and both methods give similar accu-

racy with the TCM being slightly better. Finally, we notice that the third identified frequency for the TCM undergos more change than the ERA frequency. In addition, the ERA provides the better results.

This study of the effect of noise on the identifed frequencies for the ERA and the TCM has provided us with interesting results. First of all, the identified values approach the actual values as the level of noise is decreased. The rates of convergence depend on which identification method is being used and which mode is being considered. In addition, the TCM is less sensitive to noise for the first mode, while the ERA is less sensitive for the third mode. The two methods exhibit similar sensitivity for the second mode, with the TCM performing slightly better. As the level of noise is increased further, the ERA identifies a positive real pole for the fundamental frequency, and the TCM provides bad results for the higher modes. What constitutes a higher mode depends on how many modes are participating in the response. For example, the third mode identified for three modes participating in the response would be much more in error than the third mode identified for six modes participating in the response.

6.3 Identification Spillover

Practical limitations dictate that the control of distributed structures be designed and implemented using finite order models, whereby only a subset of the modes of the structure may be actively controlled. The controlled modes may represent a reduced-order model of the realized structural model. The excitation of the residual (uncontrolled) modes caused by the controller is known as control spillover and can degrade the system performance. An analogous effect exists in the identification of modal parame-

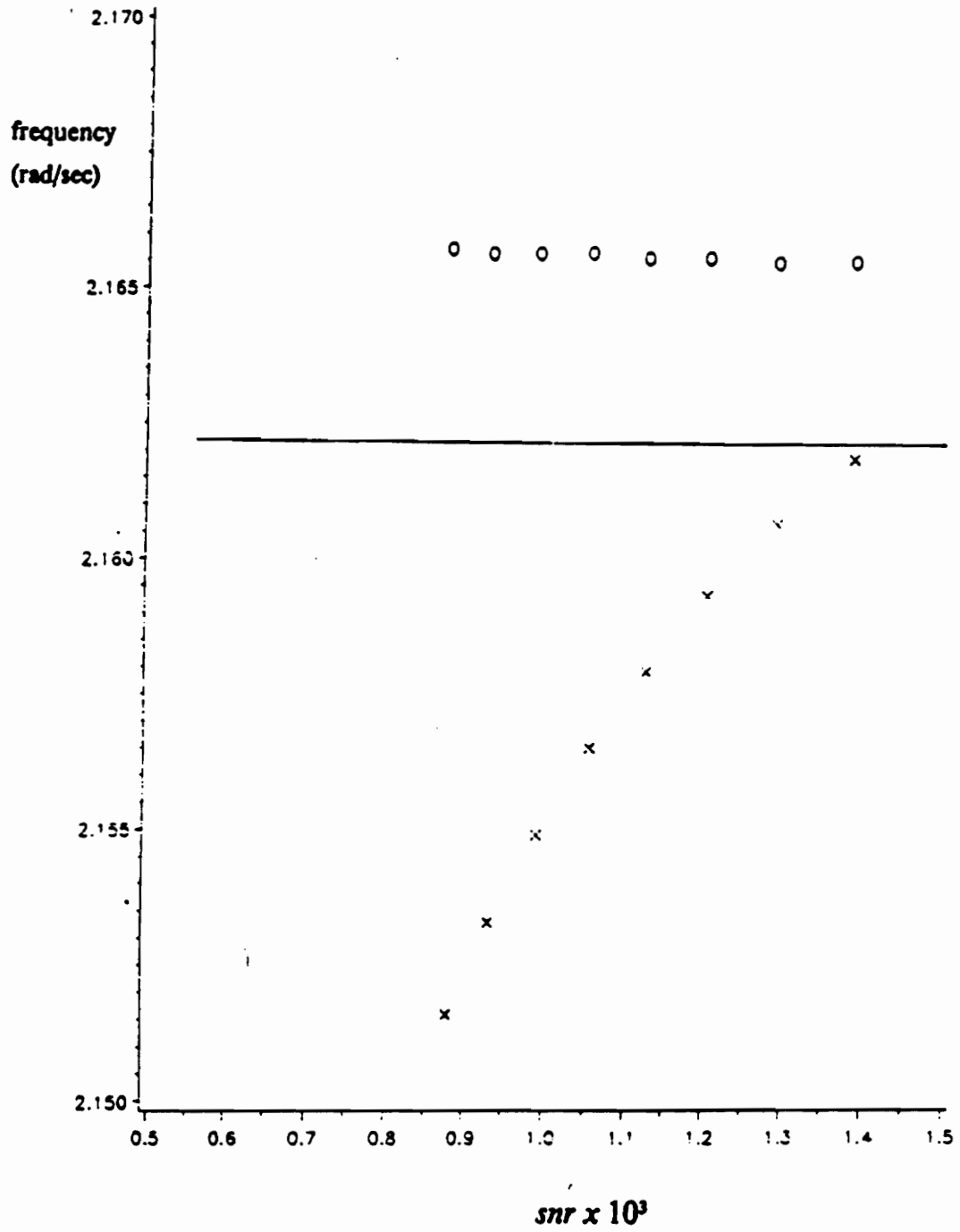

Figure 9. Effect of noise (1st natural frequency)
x-ERA, o-TCM

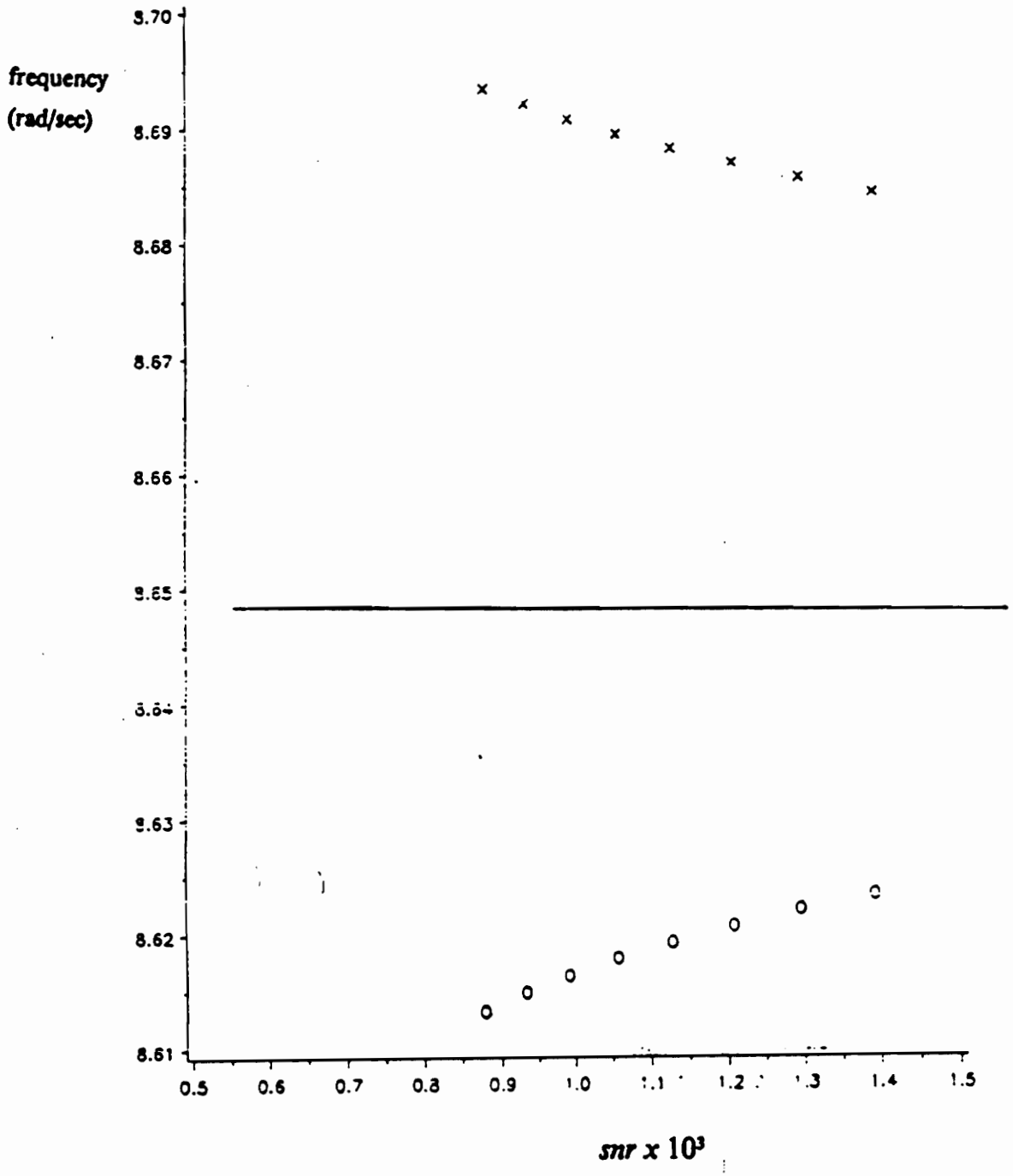

Figure 10. Effect of noise (2nd natural frequency)
x-ERA, o-TCM

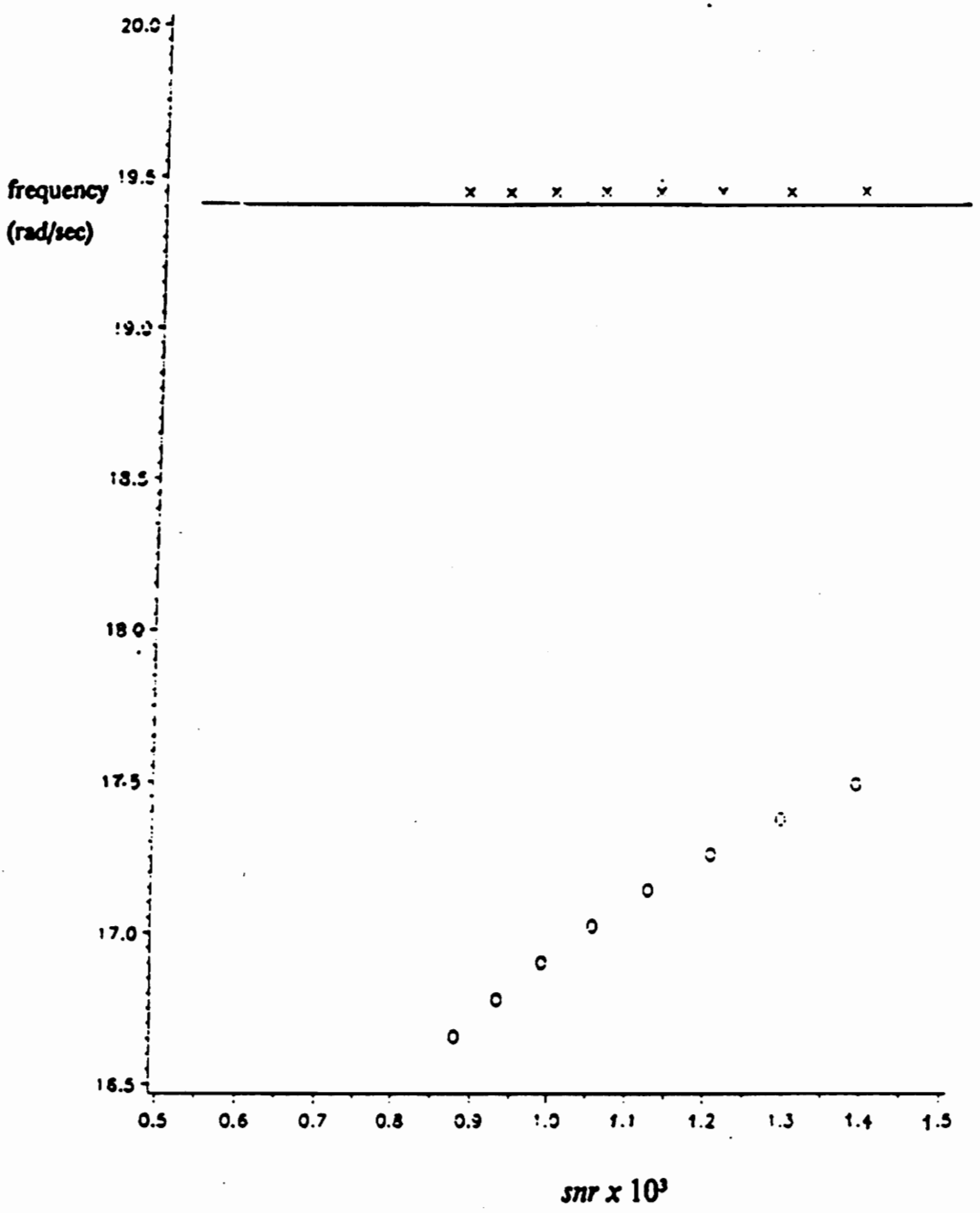

Figure 11. Effect of noise (3rd natural frequency)
x-ERA, o-TCM

ters in distributed structures. Because distributed structures must be modeled by discrete systems, the contamination from the residual (unmodeled) modes leads to identification spillover, which tends to degrade the identification results [25].

The identified eigenvalues for the TCM obey the inclusion principle. As the order of the model is increased, the identified eigenvalues approach the actual ones monotonically from above. To illustrate this and to investigate the behavior of the identified eigenvalues of the ERA, we consider once again the simply supported beam example. For this case we let the first six modes participate in the response. We implement the two methods four times, increasing the number of modes to be identified from three to six and monitor the identified frequencies. Note that for the ERA we retain $2n$ singular values, where n is the number of modes identified.

The results for the TCM and the ERA are presented in Tables 5 and 6 respectively. It is clear that the identified natural frequencies, and hence the eigenvalues, obey the inclusion principle for the TCM. Indeed, the first natural frequency for the case of three modes identified lies between the first and second identified frequencies for the case of four modes identified, and so on. The identified frequencies for the fourth and fifth modes are lower than the actual values for $m = 6$. This is inconsistent with the inclusion principle, and it is attributed to temporal truncation. The ERA estimates do not obey the inclusion principle, although the higher modes seem to be bounded. Also, we notice that the fundamental frequency is highly sensitive to spillover, with a real pole identified for $m = 4$ and $m = 5$, while the two highest modes are identified accurately for $m = 3,...,6$. This type of finding is consistent with the results of the previous sections, and would seem to indicate that the ERA is better suited to identify the higher modes.

Table 5. Identified frequencies for the TCM to illustrate spillover.

ω_r

r	n = 3	4	5	6	actual
1	3.07	2.40	2.19	2.17	2.16
2	13.29	9.88	8.88	8.66	8.65
3	55.62	36.38	23.68	19.47	19.46
4	-----	62.82	50.35	34.58	34.60
5	-----	-----	73.15	54.04	54.06
6	-----	-----	-----	77.85	77.84

Table 6. Identified frequencies for the ERA to illustrate spillover.

ω_r

r	n = 3	4	5	6	actual
1	.79	*	*	2.16	2.16
2	53.88	8.87	8.90	8.65	8.65
3	77.58	53.93	32.46	19.46	19.46
4	-----	77.70	53.96	34.60	34.60
5	-----	-----	77.73	54.06	54.06
6	-----	-----	-----	77.84	77.84

* identified real pole

It would seem as though both methods have their own advantages with respect to identification spillover. On the one hand, the TCM natural frequencies obey the inclu-

sion principle so that the identified values approach the actual ones from above. On the other hand, the ERA can provide estimates of the higher natural frequencies when only a subset of the participating modes are modeled. In other words, the higher modes that are identified are not adversely affected by the residual modes. The results presented here to illustrate identification spillover and the inclusion principle used simulated data. Experimental verification of these phenomena for the TCM and the ERA will be discussed in the next chapter.

6.4 Demonstration of the Constrained ERA

Let us consider an example of the CERA and illustrate how it relates to the TCM and the ERA. Consider a simply supported beam of uniform properties $L = 10m$, $EI = 20Nm$, and $m = 1kg/m$ undergoing bending vibration. The natural frequencies are

$$\omega_r = \sqrt{20}\,(\frac{r\pi}{10})^2 \tag{53}$$

and the normalized mode shapes are

$$\phi_r(x) = \sqrt{\frac{1}{5}}\,\sin(\frac{r\pi x}{10}) \tag{54}$$

Consider the case in which the six lowest modes participate in the response, and we wish to identify the eigenvalues corresponding to the first three. Six acceleration measurements are used at the measurement stations $x_i = iL/7 (i = 1,2,...,6)$ for this example. The response of the beam is obtained by applying an impulse at $x = 2L/7$. We compare

the identified eigenvalues for the ERA, the TCM, and the CERA. The number of sample points in correlating the measurements in the TCM is much greater than that used for the CERA due to the lengthy amount of time needed to perform the singular value decomposition on large matrices.

Table 7 contains the results for the case of no damping in the response and no noise added to the outputs. We can see that the results for all three methods are in close agreement with the actual values. The second identified frequency for the CERA has the most error, but it is still within 3% of the actual value. The third identified frequency is the most accurate.

Table 8 contains the results for the case of damping at $\zeta = .02$ and no noise. In this case the identified values for the CERA begin to deviate from the actual values. This method is highly sensitive to the level of damping. Now we find that the first identified frequency incurs the most error, with a 6.3% change from the undamped case. As we increase the damping further, all of the identified frequencies for the CERA degenerate. In fact, when we take $\zeta = .05$, the estimate for the fundamental frequency has a 23% change from the undamped case. It is interesting to note that the first and second identified values are greater than the actual ones, while the third identified value is less than the actual one. In addition, the accuracy of the CERA improves as the mode number is increased. In other words, the lowest mode is most sensitive to damping.

Finally, Table 9 contains the results for $\zeta = .02$ and Gaussian noise added to the sensor outputs such that $\eta = 2\%$. We notice that both the ERA and the TCM still give good results for all three modes, with the largest deviation being 5.7%. Also, the identified natural frequencies given by the ERA are better than those obtained by the TCM. The identified frequencies for the CERA are also consistent with the actual values, although the estimates for the first two modes are worse than those for the TCM or the

ERA. On the other hand, the CERA estimate for the third mode is much better than the corresponding TCM estimate.

Table 7. Identified frequencies to illustrate the CERA with ζ = 0, η = 0%

r =	ω_r-TCM	ω_r-ERA	ω_r-CERA	ω_r-actual
1	.442	.441	.434	.441
2	1.767	1.766	1.722	1.766
3	3.974	3.972	3.972	3.972

Table 8. Identified frequencies to illustrate the CERA with ζ = .02, η = 0%

r =	ω_r-TCM	ω_r-ERA	ω_r-CERA	ω_r-actual
1	.441	.441	.463	.441
2	1.757	1.766	1.803	1.766
3	3.927	3.972	3.943	3.972

Table 9. Identified frequencies to illustrate the CERA with ζ = .02, η = 2%

r =	ω_r-TCM	ω_r-ERA	ω_r-CERA	ω_r-actual
1	.441	.442	.474	.441
2	1.760	1.766	1.800	1.766
3	3.760	3.973	3.966	3.972

Norris [24] has performed a more extensive development of the CERA and has given results for more examples including a membrane problem. His results show a better performance for the CERA than has been depicted here. The CERA gives good results for levels of low damping and low noise. If these levels are increased, however, the first identified frequency degenerates, while the higher ones are still good. In addition, it seems that the CERA is more sensitive to damping than to noise. This is opposite of what was found for the TCM and the ERA. An important distinction to be made is that the TCM uses both accelerations and velocities in its formulation, while the ERA and the CERA use only accelerations. For simulated cases we can normally use exact velocity profiles. However, in real applications the acceleration profiles may have to be integrated to obtain the velocity profiles. This could be a source of additional error in experimental results.

7 Experimental Results: Identification of a Flexible Grid

7.1 Introduction to the Grid System

The results presented so far have used numerical simulations. In this chapter the TCM and the ERA will be implemented using experimental data from an actual system. In particular, we consider a flexible grid consisting of nine thin aluminum strips as depicted in Fig. 12. The grid is cantilevered at the top to an I-beam that is mounted to a large, highly-stiff concrete slab. The experimental setup is located at the Astronautics Laboratory at Edwards Air Force Base.

The aluminum grid was one of several elements that comprised the system. In order to measure the response of the grid, piezoelectric accelerometers (Endevco Model 7751-500) were mounted to the grid at various locations. Due to the nature of these accelerometers, these locations were limited to places on the grid where the strips overlapped. A total of eleven accelerometers were available for use. In addition the system

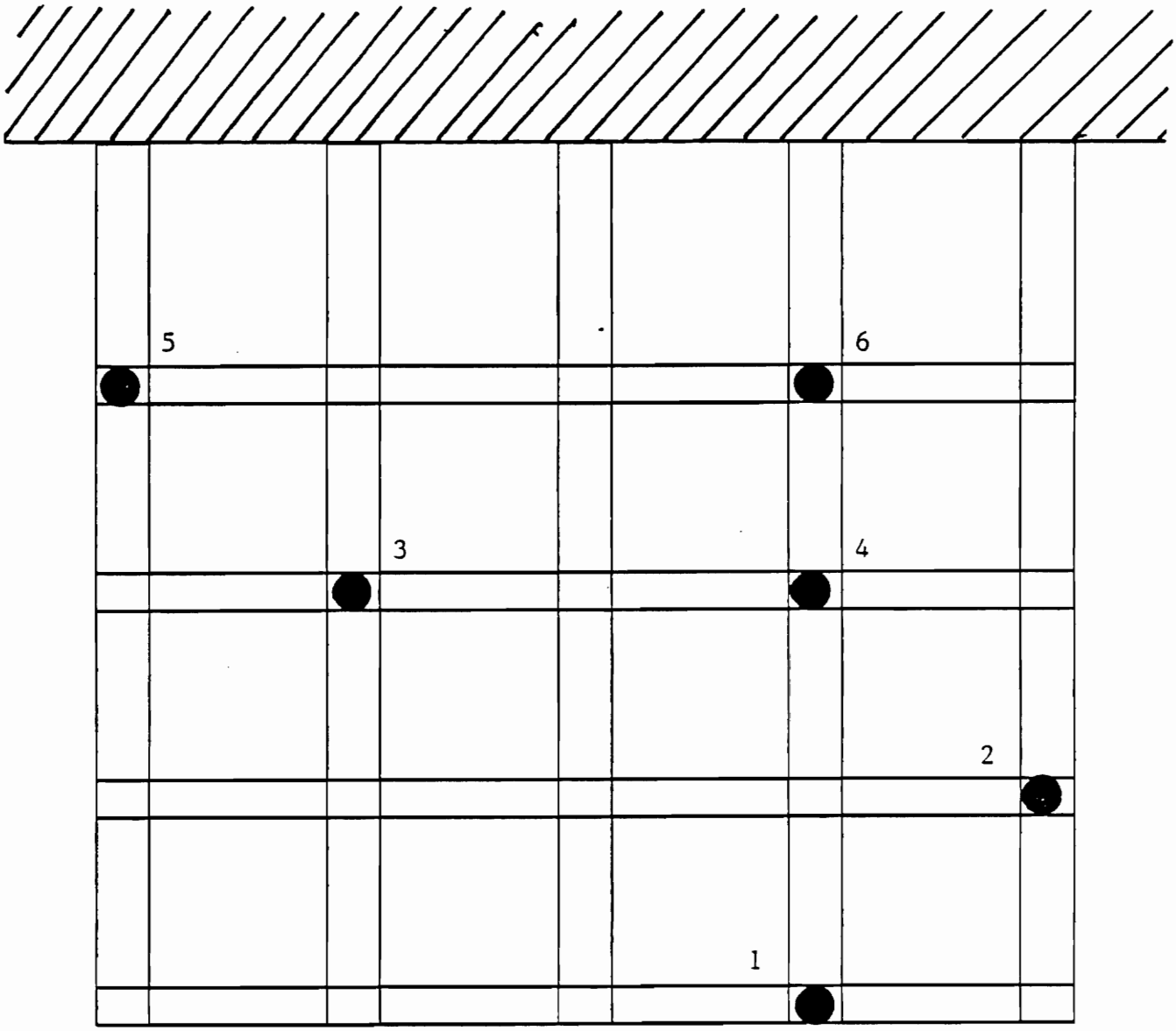

Figure 12. The AFAL Grid.

consisted of a MAX_100 central computer for data storage, a VT220 computer terminal that provided a link to MATRIXx software, and various electrical connectors. The grid was initially excited by manually shaking it. Because this often produced noise and excited the higher modes, it was usually necessary to wait ten seconds before measuring the response. In all cases the sampling frequency used was 200 Hz.

Many sets of data were taken, each one differing in the way it was shaken, where the accelerometers were located, how many samples were taken, or how much time passed between the excitation and the data collection, which we call the collection lag. In theory, the greater the collection lag the better the results will be for both the TCM and the ERA. Note that the higher modes damp out more quickly, leaving only the lower modes to participate in the response, so that the effect of identification spillover is decreased.

7.2 Modal Identification of a Grid

In this section we implement the TCM and the ERA on the grid structure, and we compare the results. The frequency response plots of the different sets of data can be viewed to determine which set was the "cleanest". It was found that this data set was characterized by 4,096 samples with a total collection time of T = 20.48 s. In addition, the accelerometers were placed at points as depicted by Fig. 12. The six accelerometers that were used were taken from the total of eleven accelerometer measurements based on the sharpness of the peaks in the corresponding frequency response plots. The time and frequency responses of the six accelerometers chosen are shown in Figs. 13-18.

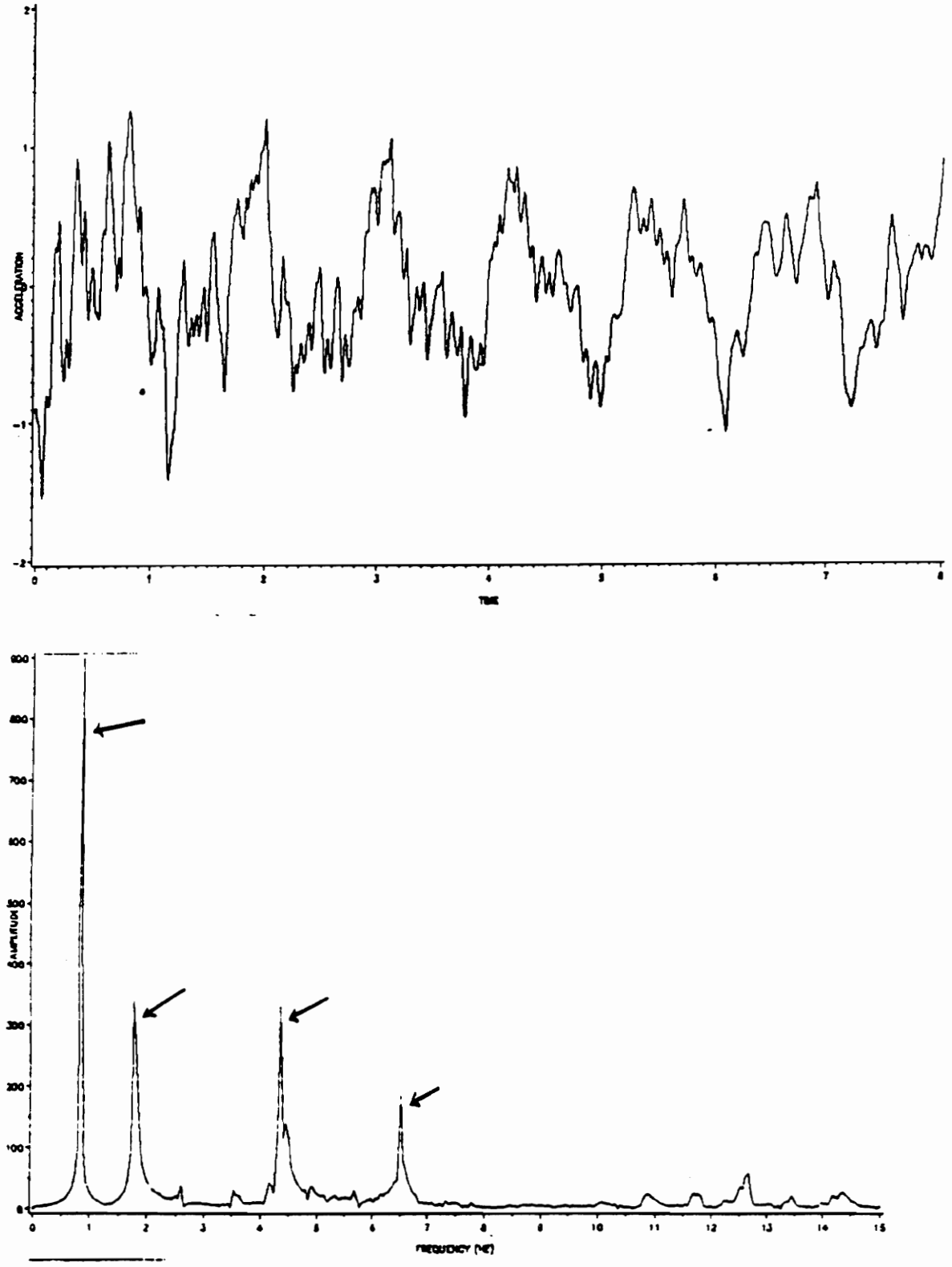

Figure 13. Time and frequency responses of the grid (accelerometer no.1)

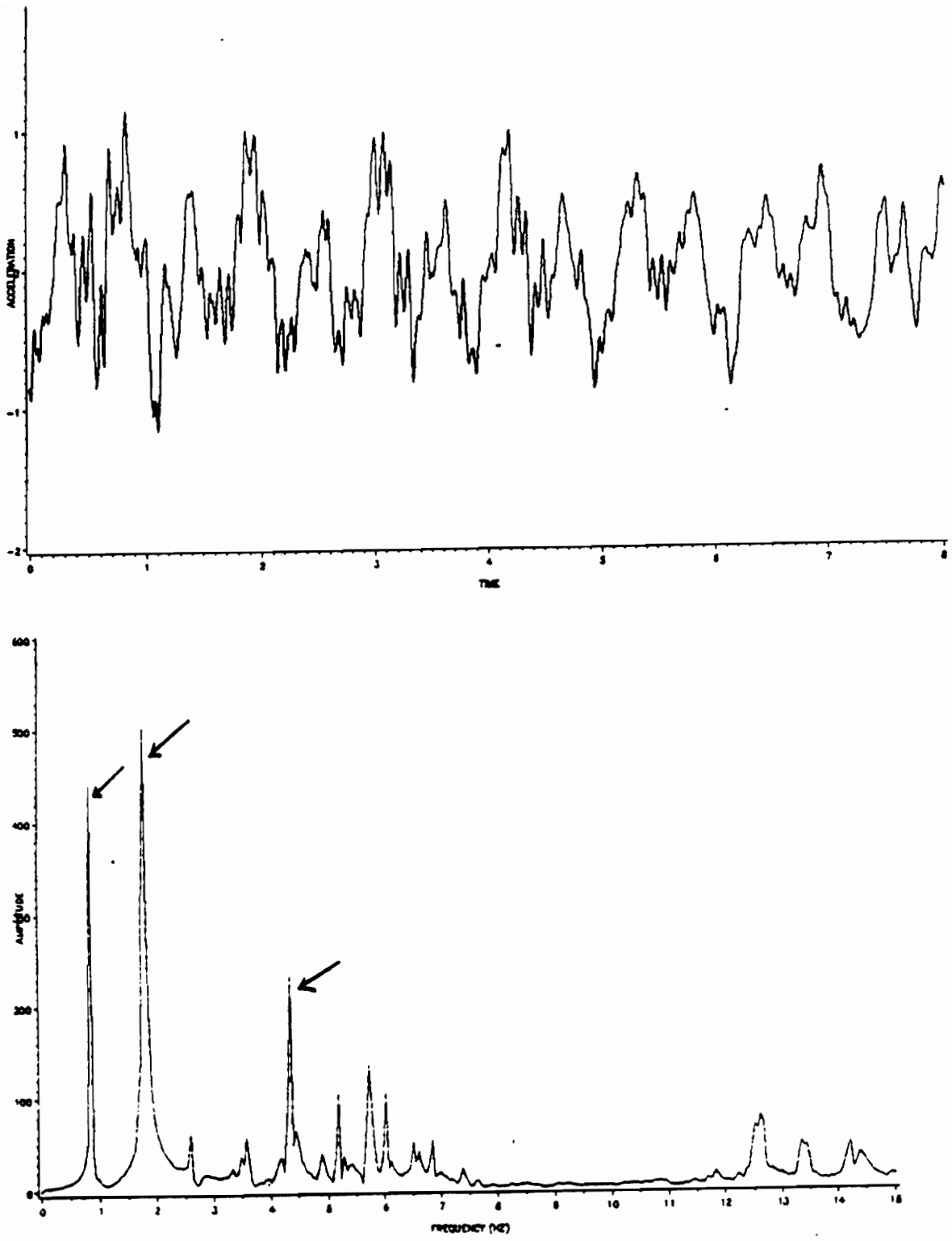

Figure 14. Time and frequency responses of the grid (accelerometer no.2)

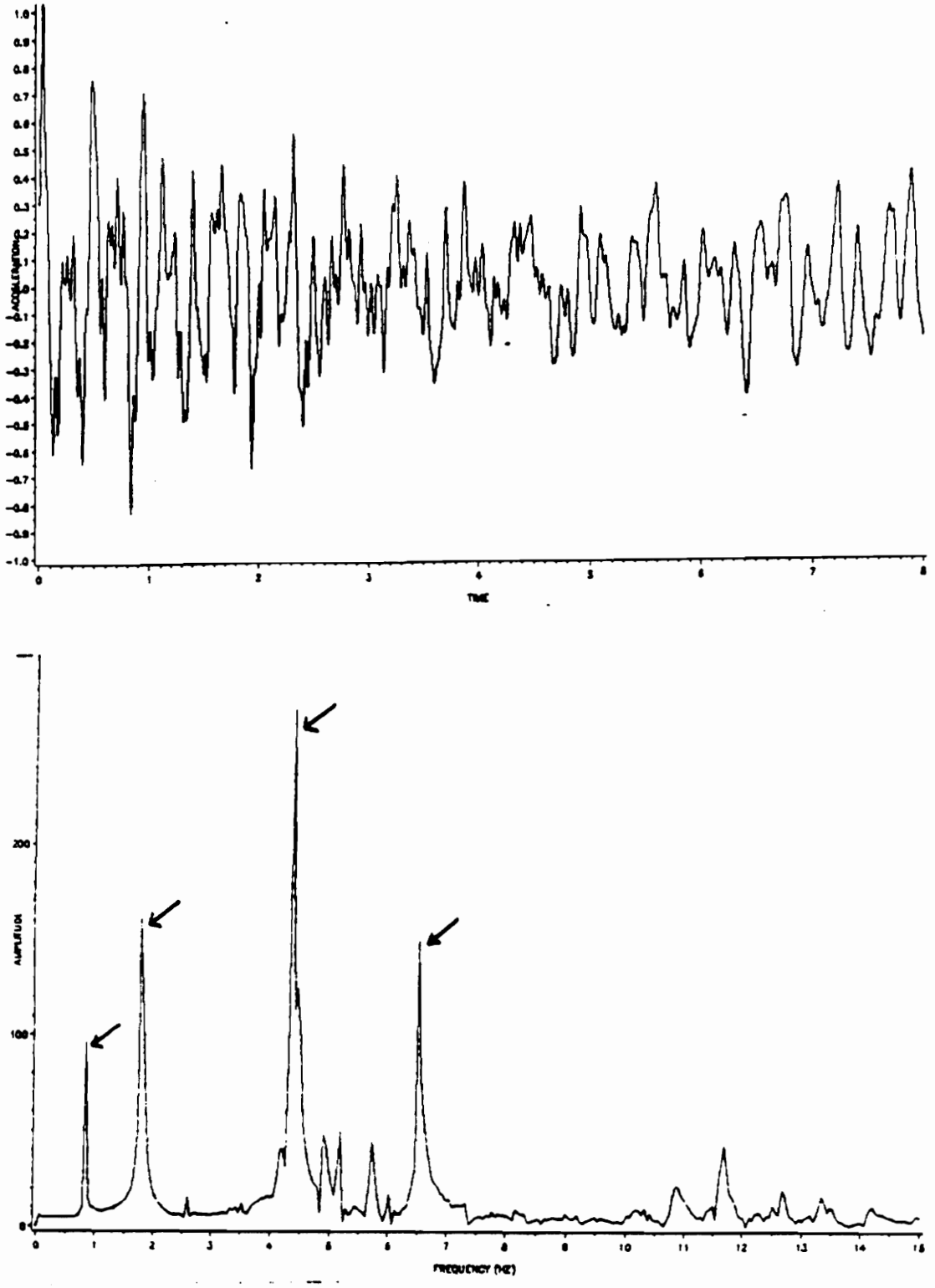

Figure 15. Time and frequency responses of the grid (accelerometer no.3)

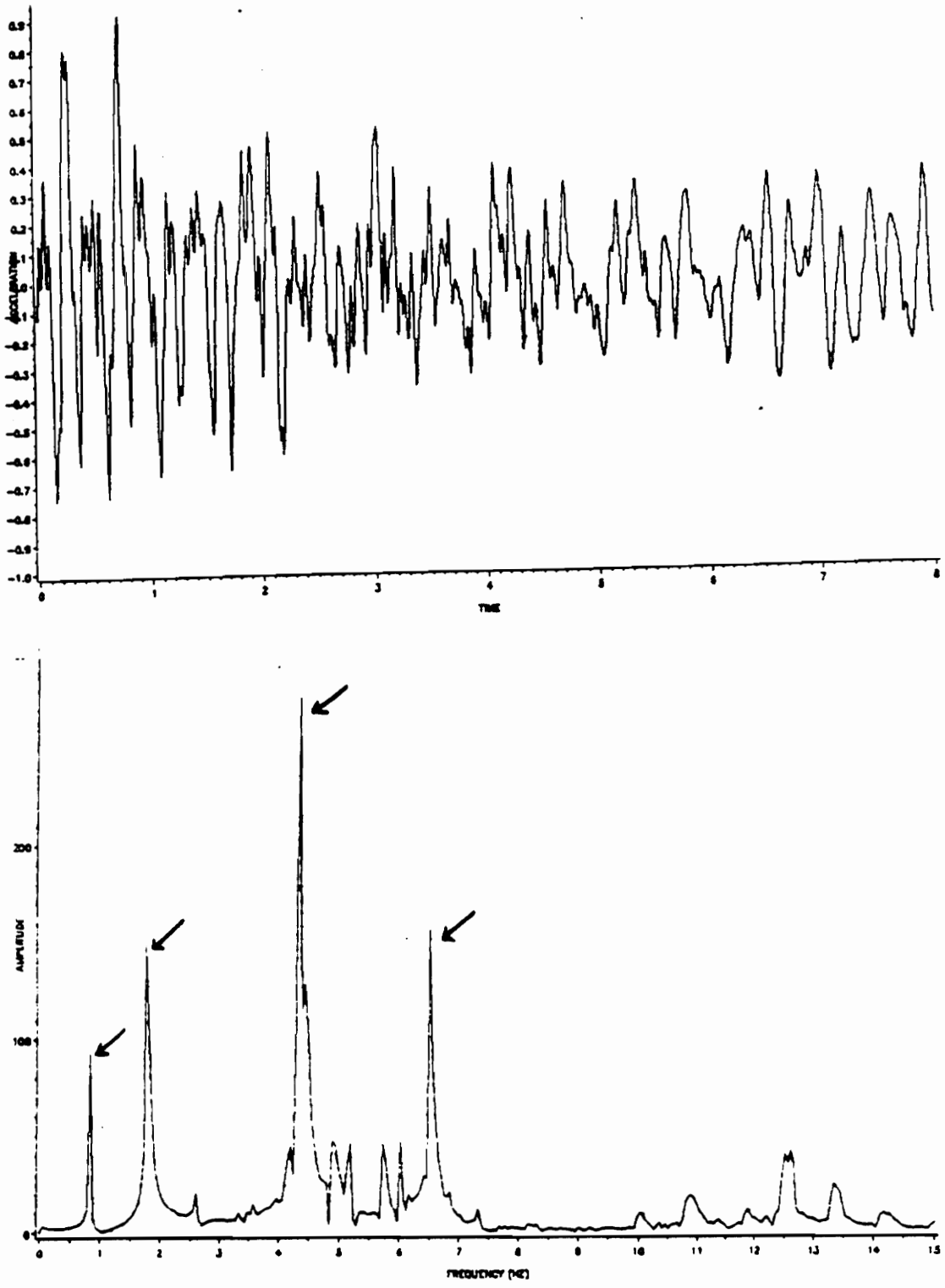

Figure 16. Time and frequency responses of the grid (accelerometer no.4)

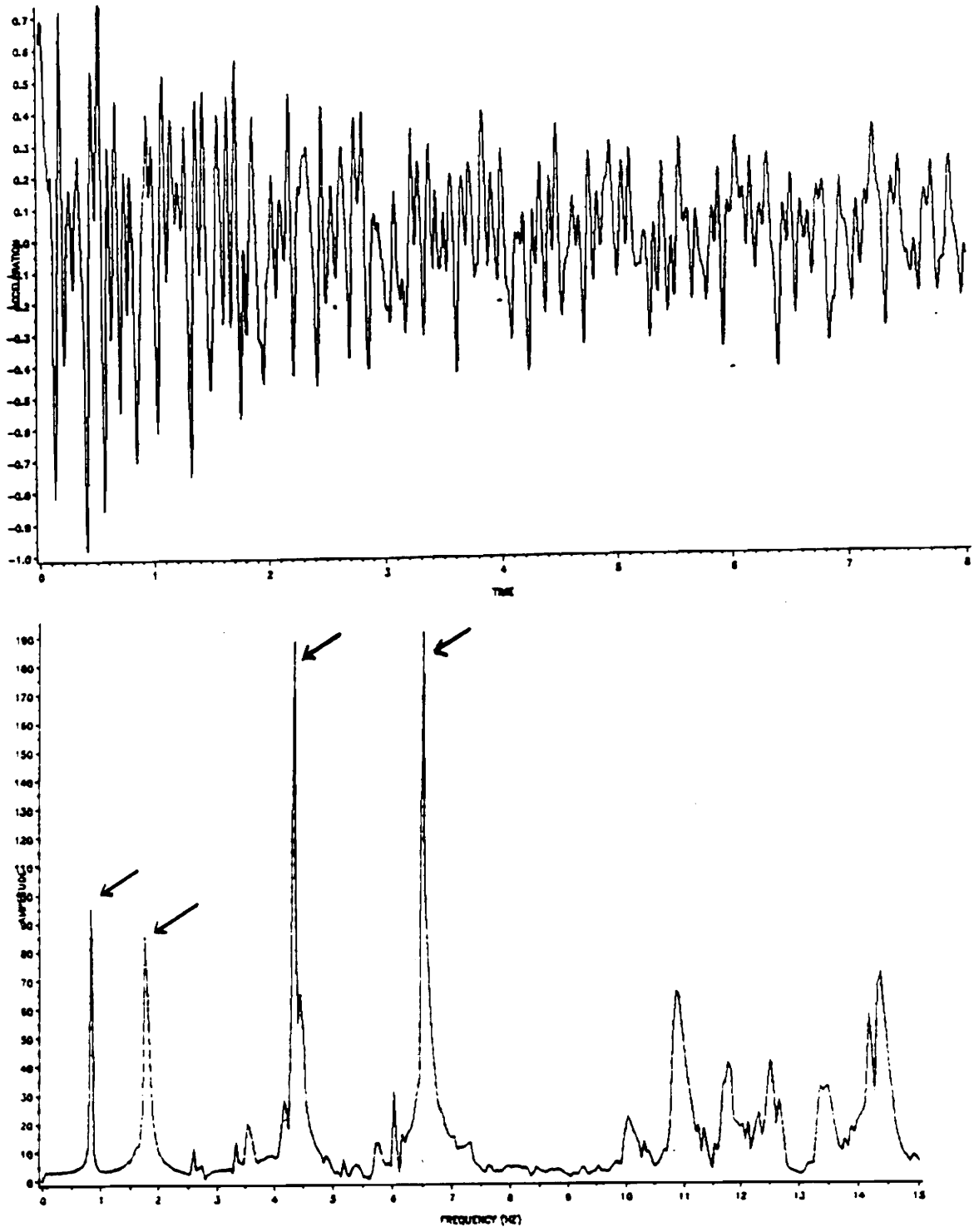

Figure 17. Time and frequency responses of the grid (accelerometer no.5)

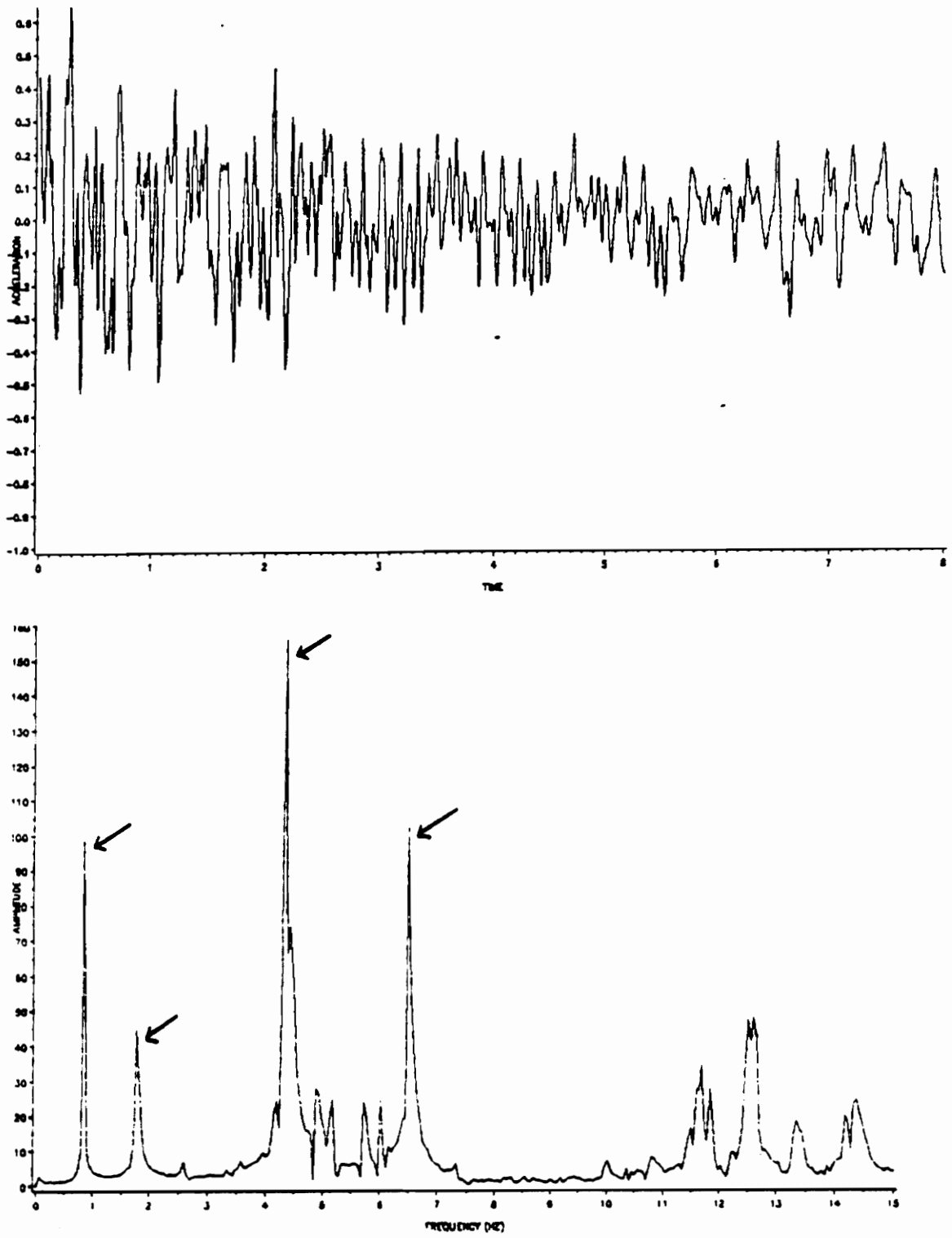

Figure 18. Time and frequency responses of the grid (accelerometer no.6)

Table 10 contains the identified frequencies corresponding to the first four modes of the grid for both the TCM and the ERA. The size of the Hankel matrix for the ERA is defined by the parameters $r = 36$, $l = 4$, $s = 100$, and $m = 1$ in Eq. (34). Actual raw data was used, meaning that no filtering was performed. In addition, Table 10 contains the estimated values of the first four frequencies of the grid which were obtained through inspection of the frequency response plots of the accelerometer outputs. Due to the varying nature of the frequency response plots for six accelerometers, the estimated values were taken to be an average of the more distinct peaks at different frequencies. These peaks are indicated by an arrow in the figures. We note that the results for the TCM on the first, second, and fourth modes are good, while the results for the third mode is in considerable error. Also, the ERA results are not accurate, except that the second and third identified frequencies correspond well to the third and fourth estimated frequencies.

Table 10. Identified frequencies of a grid (no filtering)

r =	ω_r-TCM	ω_r-ERA	ω_r-est.
1	.93	1.38	.83
2	2.01	4.44	1.76
3	3.32	6.54	4.35
4	6.36	13.14	6.49

In order to improve the results for the two methods, we consider filtering the data. The process consisted of performing a Fast Fourier Transform (FFT) of the accelerometer outputs, setting to zero all terms past a selected frequency, and performing an inverse FFT to return to the time domain. Table 11 displays the identified values for the first four natural frequencies using the TCM and the ERA after the acceleration data had been filtered with a cutoff frequency of 10 Hz. The filtered time domain response plots are shown in Figs. 19, 20, and 21, and we note that the time histories are smoother than for the unfiltered cases (Figs. 13-18).

Table 11. Identified frequencies of a grid (filtered at 10 Hz)

r =	ω_r-TCM	ω_r-ERA	ω_r-est.
1	.86	.78	.83
2	1.79	2.46	1.76
3	2.52	4.34	4.35
4	5.98	6.55	6.49

We can see that the results for both methods have improved drastically. Both methods identify the fundamental frequency, often the one of greatest interest, extremely well. It is also evident, however, that the TCM has trouble with the higher two modes, while the ERA has trouble with the second mode. In addition, we find a similar pattern

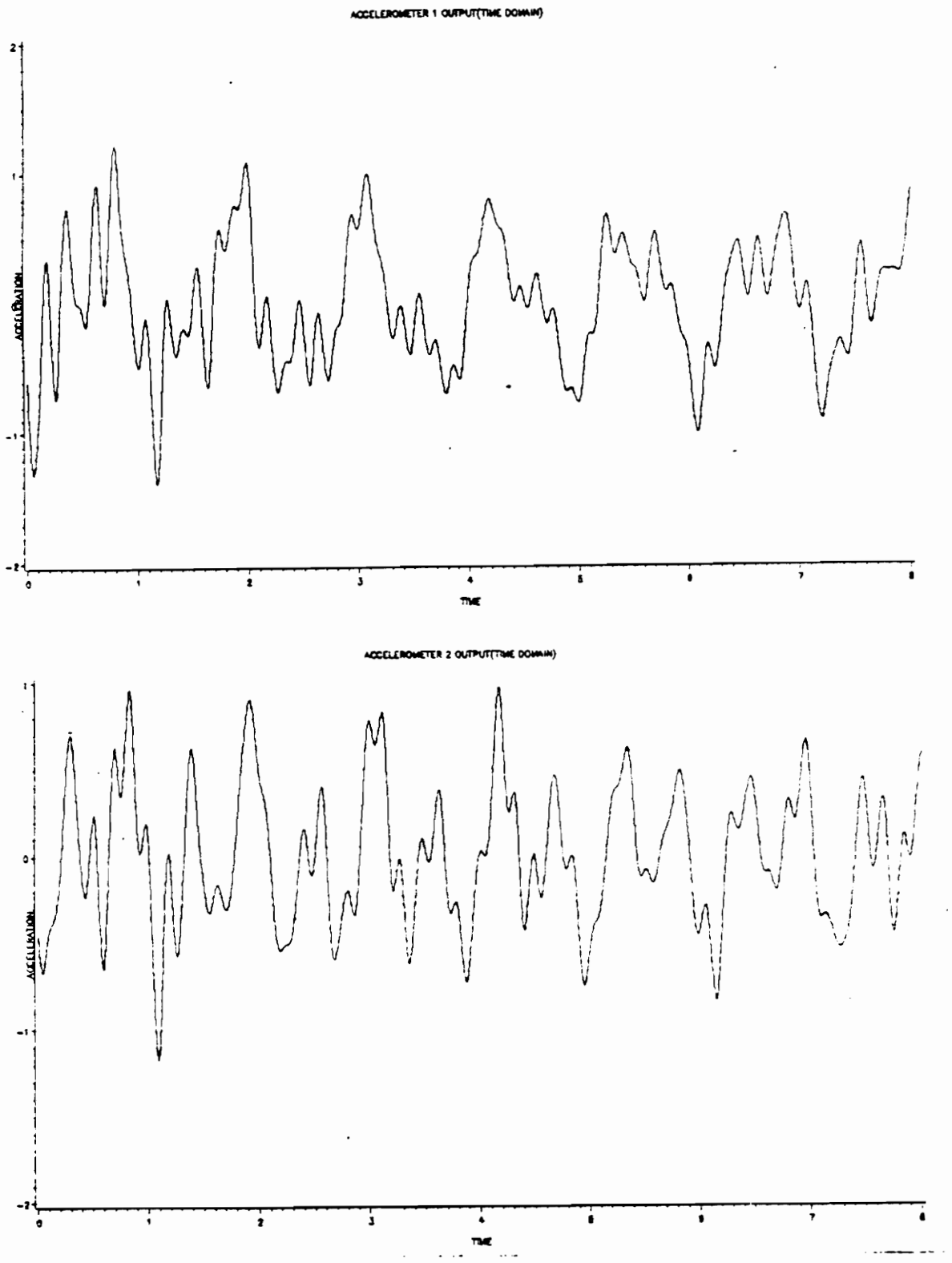

Figure 19. Filtered time responses of the grid (accelerometer no.1 and no.2)

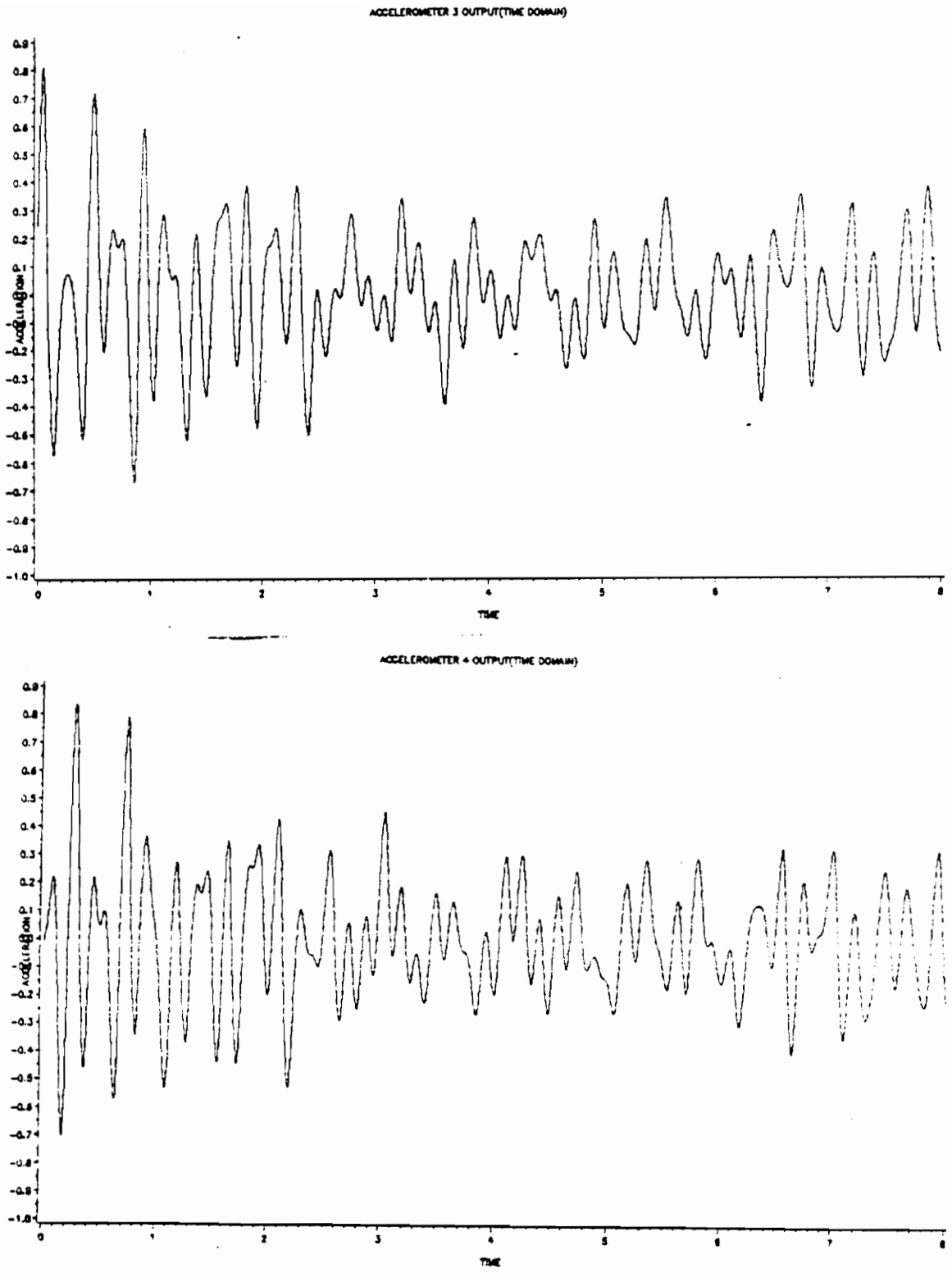

Figure 20. Filtered time responses of the grid (accelerometer no.3 and no.4)

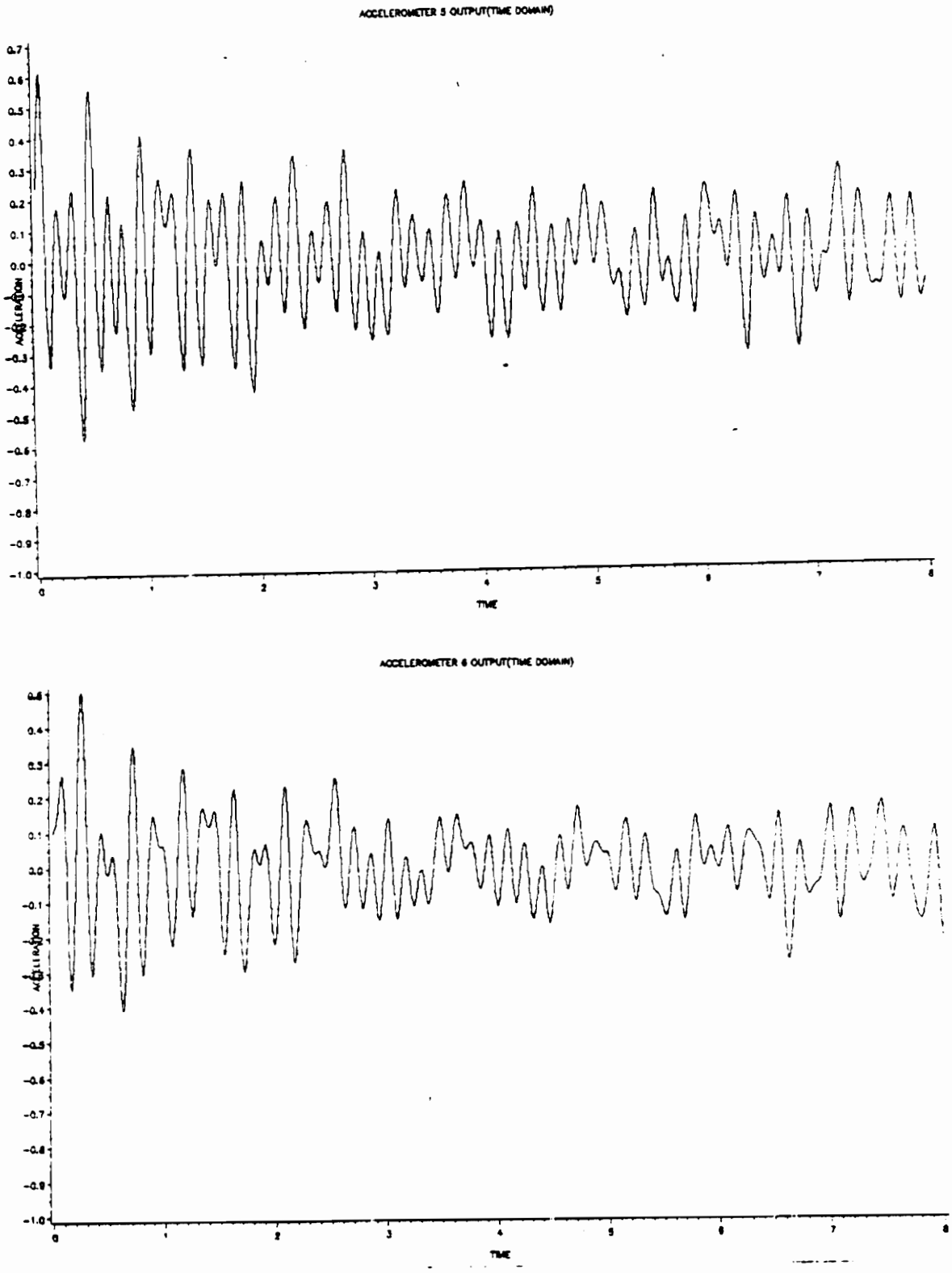

Figure 21. Filtered time response of the grid (accelerometer no.5 and no.6)

exhibited by the simulation results of the previous chapter. In particular, the TCM is more accurate for the lower modes, while the ERA performs better for the higher modes.

Considering again the frequency response plots, we notice that the last distinct peak occurs at approximately 6.5 Hz. To reduce the effect of noise and identification spillover further, we implement the TCM and the ERA again using a data set filtered at 7.5 Hz. Table 12 contains the identified frequencies along with the estimated values. The numbers in parenthesis represent the percent change from the filtered case at 10 Hz.

Table 12. Identified frequencies of a grid (filtered at 7.5 Hz)

r =	ω_r-TCM	ω_r-ERA	ω_r-est.
1	.86 (0.0)	.84 (65.0)	.83
2	1.78 (1.1)	1.96 (7.4)	1.76
3	2.52 (0.0)	4.43 (3.3)	4.35
4	5.96 (0.3)	6.55 (0.0)	6.49

Based on these results and a comparison to Table 11, it is clear that the additional filtering did not improve the results. In fact, for the fundamental frequency identified by the ERA, the accuracy was drastically reduced. Another interesting observation is that the identified frequencies for the TCM are hardly affected by the additional filtering. These results serve to illustrate that the success of this type of filtering process on the ERA identified frequencies is highly dependent on the cutoff frequency. What value to

use is not an easy question to answer, however, so that care must be taken when performing this step.

To improve the results for the ERA, we consider using several data sets. This is done by splitting up the original set of data into three subintervals, and by taking each subinterval as an independent data set with different initial conditions. Table 13 compares the estimated frequencies with those obtained by the ERA using the parameters $r = 36$, $l = 4$, $s = 100$, and $m = 3$. In addition, the results from the single data set are repeated for comparison. The first two identified frequencies show an improvement from the use of multiple data sets. Conversely, the third and fourth identified frequencies either degenerate or remain unchanged. Overall, however, it appears that improved results are obtained by including multiple data sets. It should be noted that the improved results are not without cost. Using multiple data sets, more computer time is required in both constructing the Hankel matrix and in performing the singular value decomposition.

Table 13. Identified frequencies of a grid using multiple data sets for the ERA.

r =	ω_r-ERA (m = 1)	ω_r-ERA (m = 3)	ω_r-est.
1	.78	.84	.83
2	2.46	1.96	1.76
3	4.34	4.43	4.35
4	6.55	6.55	6.49

In summary, the TCM and the ERA were implemented on a grid structure, with moderate results obtained for raw data. The data was then filtered at 10 Hz, with im-

proved results, but additional filtering at 7.5 Hz caused the ERA estimates to degenerate. Hence, filtering is beneficial to the identification process, but the methods may be sensitive to the cutoff frequency chosen. Finally, the ERA was implemented using multiple data sets with slightly improved results.

7.3 Identification Spillover

In section 6.3 we investigated the effect of identification spillover on the identified natural frequencies for both the TCM and the ERA. It was found that the identified frequencies for the TCM obey the inclusion principle and that the higher modes for the ERA are not greatly affected. These conclusions were based on a simulated example of a simply supported beam. Now consider the effect of identification spillover on these two methods using accelerometer data from the grid. The data was filtered at 10 Hz so that four modes predominantly participate in the response. This can be seen by inspection of Figs. 13-18.

Table 14 contains the results for identifying two, three, and four modes using the TCM. Note that the number of sensors used is equal to the number of modes to be identified. Once again it is clear that the identified natural frequencies obey an inclusion principle. The identified frequencies for the third and fourth modes are less than the estimated values. We attribute this to sensor noise and truncation of the temporal inner product. For the simulated case, the first identified frequency deviated significantly from the actual value as the number of modes identified decreased. For the grid data, this was not the case. Note that even when two modes are identified, the first identified frequency is a good estimate of the actual fundamental frequency. This discrepancy

arises because for the simulated case more modes were participating in the response so that the effect of identification spillover was more pronounced.

Table 15 contains similar information for the identified frequencies using the ERA. The parameters used were $r = 48$, $l = 4$, $s = 150$, and $m = 1$. Again we notice that the higher identified frequencies (excluding the first) are good approximations to the higher modes participating in the response. For example, when three modes are identified, the second and third frequencies are 4.42 rad/sec and 6.58 rad/sec. Comparing this to the estimated values for the third and fourth natural frequencies of 4.35 rad/sec and 6.49 rad/sec, we see there is a direct correspondence. For this case we do not identify a positive real pole such as those obtained for the simulated data. In addition, it appears that all of the identified frequencies obey an inclusion principle, not just the higher ones.

Table 14. Effect of ID spillover using grid results for the TCM.

	ω_r			
r	n = 2	3	4	estimated
1	.93	.87	.86	.83
2	2.29	2.22	1.79	1.76
3	----	4.99	2.52	4.35
4	----	----	5.98	6.49

Table 15. Effect of ID spillover using grid results for the ERA.

	ω_r			
r	n = 2	3	4	estimated
1	1.36	.97	.78	.83
2	4.55	4.42	2.46	1.76
3	----	6.58	4.34	4.35
4	----	----	6.55	6.49

8 Conclusions

We have considered several modal identification techniques. They have been tested with computer simulations as well as with experimental data obtained from the Astronautics Laboratory Grid Experiment located at Edwards Air Force Base. The techniques used include: (1) the Temporal Correlation Method, (2) the Eigensystem Realization Algorithm, and (3) the Constrained Eigensystem Realization Algorithm.

Chapters three, four, and five provide the theoretical background for these methods. The TCM uses the temporal correlation properties of the modes of vibration, and the identified frequencies and mode shapes are found by solving an algebraic eigenvalue problem that contains matrices of correlated sensor outputs. There are requirements on the sampling interval and the total integration time needed to obtain accurate results. The ERA is formed by using the singular values of the generalized Hankel matrix to obtain a minimum order realization. Again, an algebraic eigenvalue problem is solved to obtain the identified frequencies and mode shapes. The order of the algebraic eigenvalue for the ERA is twice that of the one for the TCM. In order to improve efficiency, the CERA was introduced. This method uses only one row of block matrices in the generalized Hankel matrix, and is only valid in cases of light damping.

Chapter six provides simulation studies to demonstrate how the methods work. This includes a study of the effect of noise on the identified frequencies for the TCM and the ERA. In addition, a discussion on the effect of identification spillover is given. The results of this chapter prove interesting.

It was found in section 6.1, for the simple beam example given, that the ERA provided better estimates for the higher frequencies while the TCM gave better estimates of the lower ones. In addition, the ERA was not affected by the addition of damping, while the TCM did experience some error. A noise effect study was performed in section 6.2. The first three frequencies of a simply supported beam were identified using the TCM and the ERA as the amount of noise was varied. It was found that the identified values approach the actual values as the level of noise is decreased. The rate of convergence is dependent on the mode considered and the method used. It was also found that the the ERA lower modes and the TCM higher modes were most sensitive to the noise. Section 6.3 provided a look at the effect of identification spillover on identified frequencies of the TCM and the ERA. It was discovered that the identified frequencies of the TCM obey an inclusion principle so that the frequencies approach the actual values from above as the number of modes modeled is increase. For the ERA, it was found that the ERA provides good estimates of the higher frequencies participating in the response.

The final section of the chapter provided some simulation results for the CERA. For low levels of damping and low levels of noise the identified frequencies are in agreement with the actual frequencies. Moderate levels of either damping or noise, however, tend to degrade the results for the first mode. The higher modes are not adversely affected. Two factors can limit the amount of success obtained with this method. First of all, the number of columns in the Hankel matrix must be large enough to accurately portray the temporal inner product. If this is not the case, the identified results

will be affected. On the other hand, if the size of the Hankel matrix is too large, the singular value decomposition may become inaccurate which would in turn affect the identified results as well.

In Chapter 7 the TCM and the ERA are implemented on an actual system, namely the AFAL Grid experiment. The frequency response plots of the accelerometers were viewed to obtain the "cleanest" data for the analysis. Section 7.2 contains results for the first four identified frequencies of the grid using the TCM and the ERA. The analysis is initially carried out on raw, or unfiltered, data. The TCM provides good results for the first, second, and fourth modes, while the third mode is in error. The ERA, on the other hand, predicts second and third mode frequencies that are consistent with the estimated third and fourth mode frequencies.

The results are improved by filtering the data at 10 Hz, thereby reducing the effect of identification spillover. The TCM still exhibits difficulties with the third mode. The first and second mode results are improved, while the fourth mode result becomes worse. The ERA benefits greatly from the filtering process as the identified frequencies, with the exception of the second mode, are within six percent of the estimated ones. The results of this analysis also suggest that the ERA may be better suited to identify higher modes while the TCM may be better suited to identify the lower ones. The data is then filtered with a cutoff frequency of 7.5 Hz. The TCM shows no significant change in the identified frequencies, while the ERA results are not as good as the filtered case at 10 Hz. This suggests possible difficulties in determining a suitable cutoff frequency. Finally, the results for the ERA are improved further by considering multiple data sets. In fact, the identified frequency for the second mode improves from a 28% error to a 10% error.

In the next section we investigated the effect of identification spillover on experimental results. The results from this section were consistent with what we found from the simulated case. In particular, the identified frequencies for the TCM obey an inclu-

sion principle, so that the identified values approach the actual values monotonically from above as the number of modes modeled is increased. Noise, however, can cause the identified values to be lower than the estimates. Similar behavior is found between the simulation study of identification spillover for the ERA and the experimental study as well. In both cases the higher modes that are identified are good approximations to the higher modes participating in the response. In addition, the identified frequencies for the experimental data obey an inclusion principle in the same fashion that the TCM frequencies do.

9 References

1. Caravani, P., Watson, M.L., and Thomson, W.T., ***" Recursive Least-Squares Time Domain Identification of Structural Parameters, "*** *The Journal of Applied Mechanics* , Vol. 10, 1977, pp.135-140.

2. Smith, W.R., ***"Least-Squares Time Domain Method for Simultaneous Identification of Vibration Parameters From Multiple Free Response Records,"*** Rockwell International Corporation, STS 81-0530, 1981.

3. Wilcox, P.R. and Crawford, W.L., *A Least Squares Method for the Reduction of Free-Oscillation Data,* , NASA, TN D-4503 (June 1968).

4. Smith, W.R., *Signal Averaging and Least Squares Method for Analysis of Transient Response Data* , McDonnell Douglas Aircraft Corp., DAC-6780 (Feb. 1969).

5. Ibrahim, S.R. and Mikulcik, E.C., ***" The Experimental Determination of Vibration Parameters from Time Responses,"*** *The Shock and Vibration Bulletin* , Bulletin 46, 1976.

6. Ibrahim, S.R. and Mikulcik, E.C., *" A Method for the Direct Identification of Vibration Parameters from the Free Response,"* *The Shock and Vibration Bulletin* , No.47, Pt.4, Sept. 1977, pp.183-198.

7. Juang, J. and Pappa, R.S., *" An Eigensystem Realization Algorithm for Modal Parameter Identification and Modal Reduction,"* *Journal of Guidance, Control, and Dynamics* , Vol. 8, No. 5, Sept.-Oct. 1985, pp.620-627.

8. Pappa, R.S. and Juang, J., *" Galileo Spacecraft Modal Identification Using an Eigensystem Realization Algorithm,"* *The Journal of the Astronautical Sciences* , Vol. 33, No. 1, January-March 1985, pp.15-33.

9. Juang, J. and Pappa, R.S., *" Effects of Noise on Modal Parameters Identified by the Eigensystem Realization Algorithm,"* *Journal of Guidance, Control, and Dynamics* , Vol.9, No.3, May-June 1986, pp.294-303.

10. Juang, J., Cooper, J.E., and Wright, J.R., *" An Eigensystem Realization Algorithm Using Data Correlation (ERA/DC) for Modal Parameter Identification,"* *Control-Theory and Advanced Technology* , Vol.4, No.1, 1988, pp.5-14.

11. Juang, J. and Suzuli, H., *" An Eigensystem Realization Algorithm in Frequency Domain for Modal Parameter Identification,"* *Journal of Vibration, Stress, and Reliability in Design* , Vol.110, January 1988, pp.24-29.

12. Longman, R.W. and Juang, J., *" A Variance Based Confidence Criterion for ERA Identified Modal Parameters,"* *AAS/AIAA Astrodynamics Specialist Conference* , Kalispell, Montana, August 10-13, 1987.

13. Pappa, R.S. and Juang, J., *" Some Experiences with the Eigensystem Realization Algorithm,"* *Journal of Sound and Vibration* , January 1988, pp.30-34.

14. Montgomery, R.C., Williams, J.P., Lazarus, T.L., and Nelson, P.E., ***Control Effectiveness Characterization for State Estimation and Control on a Highly Flexible Grid,"*** *AIAA Guidance, Navigation and Control Conference* , Williamsburg, Virginia, August 18-20, 1986.

15. Montgomery, R.C. and Lazarus, T., ***Recent Developments in the Experimental Identification of the Dynamics of a Highly Flexible Grid,"*** *1987 ASME Winter Annual Meeting* , Boston, Massachusetts, December 6-11, 1987.

16. Montgomery, R.C., Shenhar, J., and Williams, J.P., *" On-Line Identification and Attitude Control for SCOLE,"* *Proceedings of the AIAA Guidance, Navigation and Control Conference* , Monterey, California, August 17-19, 1987.

17. Sparks, Jr., D.W., Montgomery, R.C., Elder, R.C., and Lennox, D.B., *" Parameter Identification for Vibration Control of SCOLE,"* *Proceedings of the 1988 ASME Winter Annual Meeting* , Chicago, Illinois, Nov.27-Dec.2, 1988.

18. Baruh, H. and Meirovitch, L., *" Parameter Identification in Distributed Structures,: Journal of Sound and Vibration* , Vol.101, No.4, 1985, pp.551-564.

19. Meirovitch, L. and Norris, M.A., *" Parameter Identification in Distributed Spacecraft Structures,"* *Journal of the Astronautical Sciences* , Vol.32, No.4, Nov.-Dec., 1986, pp.341-353.

20. Meirovitch, L. and Norris, M.A., *" A Perturbation Technique for Parameter Identification in Distributed Structures,"* *Applied Mathematical Modelling* , Vol.12, April 1988, pp.167-174.

21. Norris, M.A. and Silverberg, L.M., *" Modal Identification of Self-Adjoint Distributed-Parameter Systems,"* *23rd Annual Technical Meeting Society of Engineering Science* , University at Buffalo, Buffalo, New York, August 1986, also appeared in the *Journal of Earthquake Engineering and Structural Dynamics* , Vol.18, 1989, pp.633-642.

22. Norris, M.A., Silverberg, L.M., Kahn, S.P. and Hedgecock, C.E., *" The Temporal Correlation Method for Modal Identification of Lightly-Damped Structures,"* *Proceedings of the 7th VPI&SU/AIAA Symposium on Dynamics and Control of Large Structures* , Blacksburg, Virginia, May 8-10, 1989, also submitted for publication in the *Journal of Sound and Vibration* .

23. Hedgecock, C.E., *" Experimental Verification and a Parametric Study of the Variational Modal Identification Method,"* Thesis in Engineering, Mechanical and Aerospace Department, North Carolina State University, Raleigh, North Carolina, 1988.

24. Norris, M.A., *" A Constrained Eigensystem Realization Algorithm for Lightly-Damped Distributed Structures,"* seminar presented at the Advanced Radiation Controls Development Branch, Kirtland Air Force Base, September 1989; to be submitted for publication in the *Journal of Guidance, Control, and Dynamics* .

25. Meirovitch, L., *Computational Methods in Structural Dynamics* , Sijthoff & Nordoff, The Netherlands, 1980.

26. Daniel, J.W. and Noble, B., ***Applied Linear Algebra*** , Prentice-Hall Inc., Englewood Cliffs, New Jersey, 1977.

27. Helzer, G., ***Applied Linear Algebra w/ APL*** , Little, Brown and Company, Boston, Massachusetts, 1983.

28. Meirovitch, L., ***Elements of Vibration Analysis*** , McGraw-Hill Book Company, New York, New York, 1986.

29. Ljung, L. and Soderstrom, T., ***Theory and Practice of Recursive Identification*** , The MIT Press, Cambridge, Massachusetts, 1983.

30. Ewins, D.J., ***Modal Testing: Theory and Practice*** , Research Studies Press Ltd., Letchworth, Hertfordshire, England, 1984.

31. Davenport, W.B. and Root, W.L., ***An Introduction to the Theory of Random Signals and Noise*** , IEEE Press, New York, New York, 1987.

32. Brillinger, D.R., ***Time Series: Data Analysis and Theory*** , Holt, Rinehart and Winston, Inc., New York, New York, 1975.

10 Vita

The author was born in Washington, D.C. on December 31, 1965. He grew up in Gaithersburg, Maryland and attended Seneca Valley High School from which he graduated in 1983. He continued his education by entering a general engineering program at Montgomery County Community College in Rockville, Maryland. He transferred into the Engineering Science and Mechanics department at Virginia Tech in the summer of 1985. During his undergraduate studies he participated in the cooperative education program by working at the David Taylor Research Center's Numerical Mechanics branch. The author obtained his Bachelors degree in May of 1988 and subsequently entered the graduate program in Engineering Mechanics.